Resolving the paragenesis of gold at the Avoca VMS deposit: implications for exploration in Caledonian terranes of southeast Ireland

Sean H. McClenaghan, Foteini Drakou, and Thomas Riegler
Department of Geology, Trinity College Dublin, Dublin 2, Ireland; Irish Centre for Research in Applied Geosciences

Abstract. The Avoca Cu-Zn-Pb-Ag VMS belt in southeast Ireland comprises a SW-NE Caledonian trend of Ordovician volcano-sedimentary rocks that host over 16 Mt of sulphides (0.6% Cu) distributed in six defined orebodies. The Kilmacoo Au Zone, on the northeast extremity of the Avoca belt comprises a resource of 300,000 tonnes at 1.5 g/t Au, containing discrete phases of electrum associated with late Caledonian structures. Although historically mined for Cu, notable resources of Zn, Pb and Ag remain at Avoca, occurring as syn-sedimentary (black shale) stratiform pyritic lenses that sit conformably within the host volcano-sedimentary stratigraphy. Sulphides have been modified by early Caledonian shearing, which has resulted in ductile attenuation of sulphides during greenschist facies metamorphism. This has resulted in recrystallization of early primary pyrite with the development of meta-blastic overgrowths and discrete porphyroblasts of pyrite. Gold contents in the Avoca VMS deposit are low overall, occurring as a refractory phase in pyrite (Avg. 0.29 ppm) and arsenopyrite (0.33 ppm). Metamorphic rims are distinctly depleted in Au, indicating barren fluids associated with prograde metamorphic processes (D_1). This would suggest that the Kilmacoo Au Zone is not related to primary zonation within the Avoca VMS system, but related to a separate distinct paragenesis.

1 Geological context

Lower Palaeozoic volcanogenic massive sulphides in the Caledonian terrane of southeast Ireland offer an ideal setting for the study of complexly deformed mineral deposits, where geochemical zonation and mineral textures are discernible through the overprinting effects of orogenesis. The effects of syn-metamorphic deformation on sulphide assemblages are important for the concentration of ore resources, resulting in structural thickening and attenuation, as well as possible secondary mobilization and enrichment from later orogenic fluids. Sulphides in the Avoca District exhibit both cataclastic and fluid-assisted deformation textures, and recrystallization (coarsening) in response to variable lower to middle-greenschist facies metamorphism. This has also had an effect on mineral chemistry, with the re-equilibration of major elements in sphalerite and arsenopyrite, and the heterogeneous distribution of trace-elements across multiple phases of pyrite. Advancements in micro-analytical techniques now allow for detailed trace-element mapping of sulphide phases (pyrite), which can reveal much of the complex interplay between fluids and mineral growth, resolving the mineral paragenesis for metamorphosed VMS deposits. This project has been developed to address outstanding questions surrounding the genesis of volcanogenic massive sulphides at the Avoca Cu-Zn deposit and possible genetic links for the adjacent Kilmacoo Au occurrence. These questions have relevance to local geology and mineral resources, but also to broader questions of fluid evolution in response to Caledonian geodynamics and correlation with equivalent hydrothermal systems across the Caledonian-Appalachian transect.

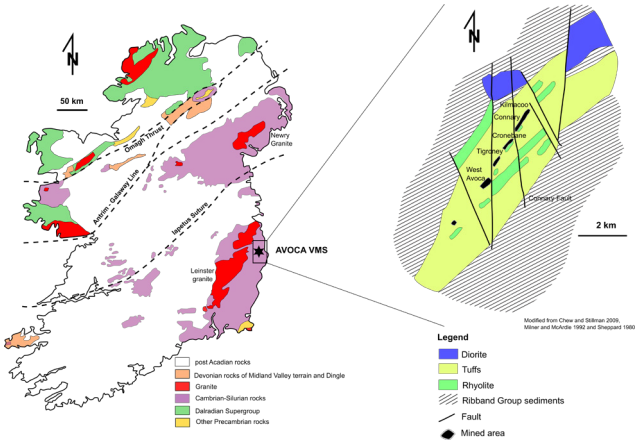

Figure 1. Simplified geological map of Ireland featuring lower Paleozoic lithologies. Inset diagram shows the distribution of sulphide orebodies.

1.1 Regional geology

Volcanogenic massive sulphides of the Avoca Belt are hosted by Ordovician volcano-sedimentary rocks of the Duncannon Group (Figure 1). These rocks were generated on an active Peri-Gondwanan margin (Iaepetus Ocean) of Ganderia, with volcanism initiated during a period of extension within a volcanic arc (Stillman and Williams, 1979; McConnell et al. 1991). The volcanic pile sits conformably to unconformably on a Cambro-Ordovician sequence of continentally-derived carbonaceous (graphitic) sediments (Ribband Group), which are exposed primarily in the Caledonian Highlands of southeast Ireland. Closure of the Iapetus Ocean resulted in the development of an accretionary wedge, with subsequent obduction and associated polyphase deformation accompanied by greenschist metamorphism.

1.2 Deposit geology

Massive sulphides at Avoca are found in both aphyric rhyodacite breccias and tuff as an epigenetic Cu-rich replacement facies and as a syngenetic exhalative massive sulphide facies in close association with black shale above the felsic volcanic pile. Orebodies have been delineated at West Avoca, Tigroney, Cronebane and Connary (Sheppard 1980; Williams et al. 1986; McArdle 1993) (Fig. 1). Massive sulphides form stratiform lenses that are coeval with their host volcaniclastic and sedimentary rocks. Their lenticular shape is in part attributed to exhalative processes. However, the aspect ratios of the ore bodies have also been affected by post-depositional poly-phase deformation. Progressive deformation has resulted in fluid-assisted remobilization and the structural attenuation of most massive sulphide bodies along the limbs of folds.

Epigenetic sulphide mineralization, comprising stringers of pyrite and chalcopyrite in siliceous veins, occurs in the footwall of the Avoca massive sulphides. Due to strong ductility contrasts between these sulphides and their host volcaniclastic rocks, stringer sulphide zones are commonly transposed parallel to the predominant S_1 composite deformation fabric. Stringer sulphide mineralization is accompanied by large alteration haloes of chlorite, sericite, silica (quartz), sulphide and carbonate, which formed through circulation of hydrothermal fluids in the footwall during massive sulphide deposition.

Metal zonation within massive sulphides is not discernible due to the thin nature of the massive sulphide lenses at Avoca. For thicker orebodies, higher temperature and lower fS_2 and pH conditions over hydrothermal vents can commonly lead to the metasomatic transformation (zone-refining) of massive sulphides into a high-temperature assemblage dominated by pyrite, pyrrhotite, and chalcopyrite. Nevertheless, a classic hydrothermal architecture does persist at Avoca, where a Cu-rich stockwork is overlain by Pb-Zn bedded sulphides and flanked by iron formation to the northeast.

1.3 Kilmacoo gold occurrence

The gold-rich Kilmacoo zone at the northeast end of the Avoca Belt (Fig. 1) is hosted by intensely sheared and altered (silica-chlorite-sericite) sulphide-rich tuffs of the Duncannon Group. Gold is associated with higher contents of pyrite, sphalerite and galena and are accompanied by a peculiar banded quartz vein unit comprising fine white to grey semi-translucent quartz (Milner and McArdle 1992). Unlike the massive sulphides to the southwest, Au is elevated in mineralization at Kilmacoo occurring as fine-grained inclusions, veins and fracture fills of native gold and electrum. The gold mineralization has broadly been interpreted as an Avoca equivalent horizon affected by late shearing (Caledonian) and influx of orogenic fluids, resulting in the enhanced gold tenor (Milner and McArdle 1992).

2 Geochemical paragenesis

Sulphides consist of pyrite, sphalerite, galena, and chalcopyrite with lesser arsenopyrite and tetrahedrite (Fig. 2). In addition, trace phases such as anglesite, stannite, chalcocite, bornite, bismuthinite, molybdenite, electrum, and a range of sulfosalts and native metals (Bi, Au, Ag), occur both as discrete phases and sub-microscopic inclusions in major phases.

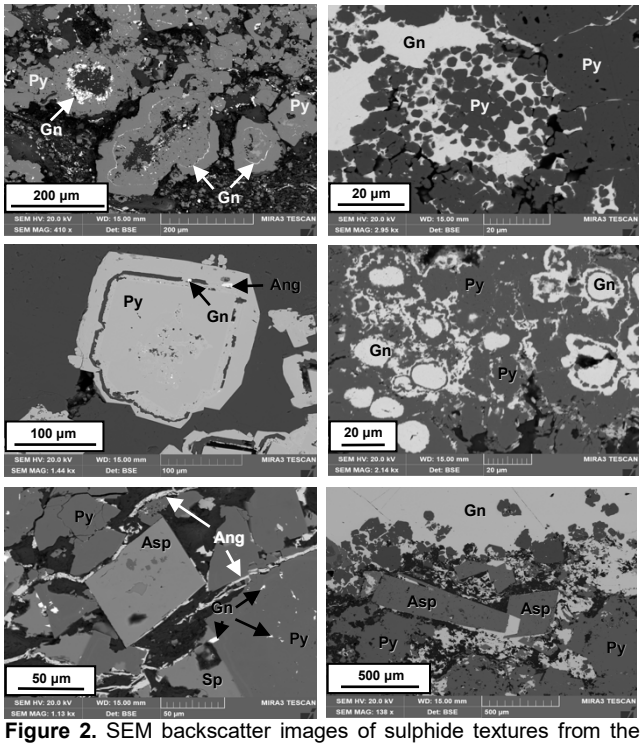

Figure 2. SEM backscatter images of sulphide textures from the Avoca Cronebane zone.

Previous studies on the mineralogy of sulphides at Avoca are sparse, and any metallurgical characterization of the ores has not been reported. Other VMS deposits hosted by Ordovician volcanic sequences have described pyrite and arsenopyrite as the principal repositories of Au in massive sulphides (McClenaghan et al. 2004; 2009), with discrete Au-bearing phases making up a small proportion of the overall mineralogical balance. Microscopic examination of sulphide minerals at Avoca was unable to establish the presence of any discrete Au-bearing phases i.e. native gold or electrum in massive sulphides or vein material. The scarcity of visible gold and electrum is not uncommon in VMS deposits and suggests gold may be present as a sub-microscopic refractory phase, or as sub-microscopic inclusions, undetectable by SEM.

Major sulphide minerals were analyzed by Laser Ablation ICP-MS in order to determine the trace element composition of the sulphide paragenetic sequence and illustrate chemical variations along their grain boundaries. Spot analyses were carried out using a spot

size of 25 µm, a fluence of 1.1 J/cm^2, 5 Hz repetition rate and a shot count of 180. Element mapping was carried out on selected mineral grains with maps generated through the ablation of overlapping 10 µm lines and processed as a continuous profile at a rate of 20 µm/sec, a laser fluence of 1.2 J/cm^2 and a 40 Hz repetition rate.

2.1 Pyrite

Pyrite at Avoca is arsenian in nature with As averaging 0.11% and ranging from as low as 15.7 ppm up to 2.15%; Arsenic exhibits a positive Spearman Rank correlation with Sb (r'=0.43; 99% confidence interval, r'>0.1). Large anhedral masses commonly exhibit zonation of As from core to rim (Fig. 3). Element mapping of a single pyrite grain reveals rhythmic growth banding of arsenic in colloform pyrite indicating the presence of lattice bound As, as opposed to inclusions of As-bearing minerals. Variations in As within the interior of the pyrite grain are likely due to fluctuating hydrothermal fluid conditions during early deposition with variable recrystallization from metamorphism. Arsenic-rich pyrite on the rim of the colloform mass is attributed to euhedral metamorphic overgrowths, which correspond to porphyroblastic growth of arsenopyrite in massive sulphides. The core of many pyrite grains can appear porous or diseased, with regions variably replaced by galena, sphalerite, chalcopyrite and sulfosalts.

Contents of Au in pyrite average 0.29 ppm and range from the detection limit to 3.9 ppm. Interestingly, Au is invariant with respect to As, suggesting gold may in part be controlled by sub-microscopic inclusions in addition to a refractory phase; a positive correlation with Ag (r'=0.67), Cu (0.62), Pb (0.51) and Sb (0.44) would support the presence of sub-microscopic inclusions of electrum. Analyses of compositionally zoned pyrite have shown that late euhedral overgrowths exhibit depletions in Au contents relative to primary forms of pyrite. Figure 3 shows increased Au within the interior of colloform pyrite; a sharp decrease in Au within the centre of the colloform mass is due to the presence of tetrahedrite at the expense of pyrite. Spatially, Au covaries with As and to a lesser degree Ag, indicating substitution into the pyrite lattice during precipitation and consistent with chemically bonded (refractory) Au in the sulphide structure.

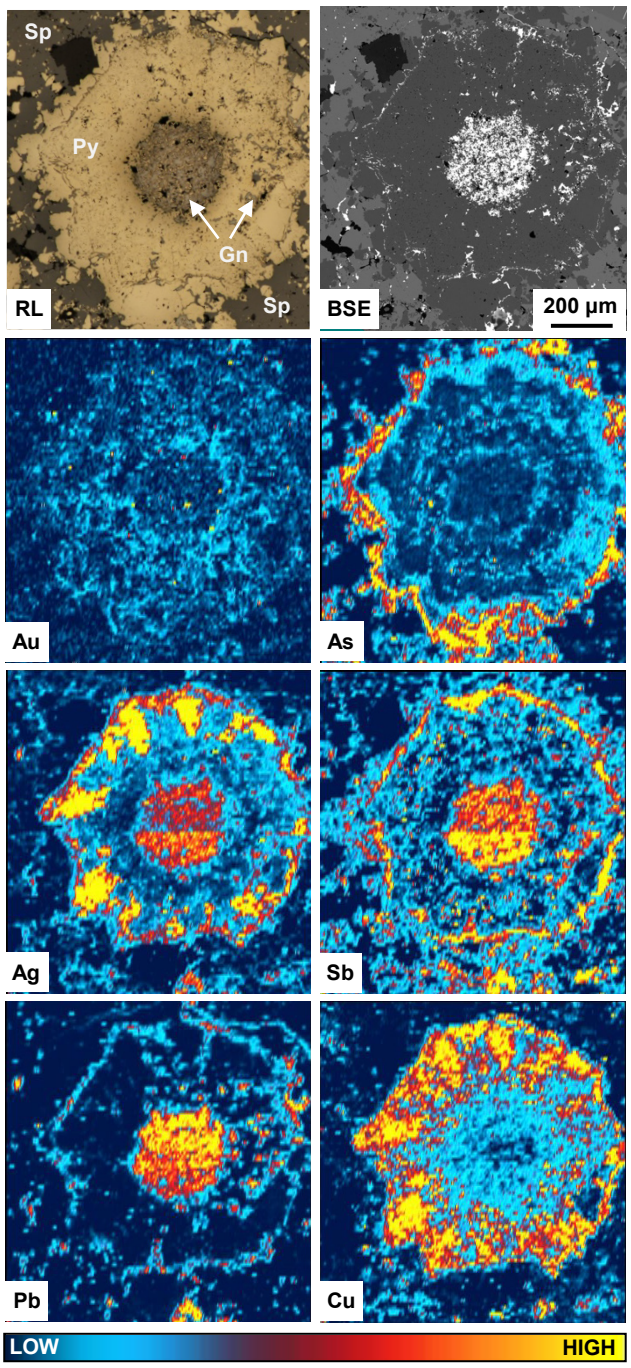

Figure 3. Laser Ablation ICP-MS element maps of a pyrite grain (Reflected Light - RL and Backscatter Electron-BSE images) from Zn-Pb banded sulphides of the Avoca Cronebane orebody. Data is semi-quantitative, displaying relative proportions of trace elements in pyrite.

2.2 Arsenopyrite

Contents of Au in arsenopyrite (n=120) are similar to pyrite, averaging 0.33 ppm, ranging from the detection limit to 2.94 ppm Au. Gold is generally invariant with respect to most hydrothermal tracer elements, exhibiting a weak positive correlation with Cu (r'=0.44; 99% confidence interval, r'>0.21). Arsenopyrite is only found in the form of porphyroblasts with its growth possibly sourcing Au from pyrite during metamorphic recrystallization. Intergrowths of arsenopyrite and pyrite are common, indicating that Au contents in arsenopyrite could be due to encroachment by surrounding pyrite inclusions. Furthermore, contents of Sb average 2313 ppm overall but vary considerably between Pb-Zn sulphides from the Cronebane pit (up to 1123 ppm Sb) and a sphalerite rich sample from the Connary zone (8900 ppm Sb). Antimony contents in arsenopyrite are refractory in nature, exhibiting a negative correlation with Zn (-0.52), Ag (-0.49) and Pb (-0.40) with inclusion of host sphalerite and galena minerals coming at the expense of Sb. Raw data for arsenopyrite spot analyses exhibit distinctive signal spikes for Pb and Ag indicating

the presence of discrete microscopic inclusions. Similarly, contents of Zn, which cover the detectable range of the instrument, including values in excess of 10% indicate inclusion of sphalerite.

3 Summary of findings

A mineralogical assessment of sulphides at the Avoca deposit indicates that Au contents in epigenetic stockwork (Cu-resource) and syngenetic exhalative sulphides (Zn-Pb-resource) are low overall. Visible gold phases (electrum, native gold) were not identified in any of the sections examined. Laser ablation ICP-MS analyses of major sulphide minerals indicate that the low gold contents in the Avoca deposit overwhelmingly occurs as a refractory phase in pyrite (Avg. 0.29 ppm) and arsenopyrite (Avg. 0.33 ppm). Given the preponderance of pyrite in massive sulphides in the VMS mineralization, the mineralogical balance of Au is hosted by pyrite. Massive sulphides at Avoca exhibit mineralogical zonation consistent with a vertically zoned hydrothermal architecture. The large Cu-resource comprising epigenetic stockwork sulphides and Cu-rich massive sulphides are stratigraphically overlain by banded Zn-Pb sulphides. An exhalative origin is ascribed to this Py-Sp-Gn facies due to its association with black shale and strong layered appearance representing pseudo-bedding that has been modified by syn-metamorphic deformation (D_1). Although massive sulphides at Avoca have been extensively modified by the effects of ductile remobilization during early shearing, primary Au signatures are largely unaffected by metasomatism. The core of primary colloform pyrite masses contain higher Au contents than late euhedral rims, which have grown and annealed in response to greenschist facies metamorphism. This suggests that prograde metasomatism was not a significant source of Au-bearing hydrothermal fluids in the region. The Zn-Pb sulphides at Kilmacoo appear to be an equivalent exhalative facies to massive sulphides outlined along strike at the Cronebane and Connary. The auriferous banded quartz unit at Kilmacoo is intercalated with the massive Zn-Pb sulphides and appears to have undergone the same syn-metamorphic deformation seen in the adjacent deposits. However, upon closer examination, the banded quartz units are seen to be cutting the early penetrative fabrics which postdate sulphide deposition and structurally modify their distribution. This indicates that Au has not been concentrated during the synthesis of VMS mineralization, but is instead related to post-D1 cross-cutting shear structures.

Addressing issues surrounding the extent of late-orogenic Au enhancement of syngenetic massive sulphides has far-reaching implications for exploration strategies along the entire Avoca Trend. The disparate styles of mineralization between the Avoca Cu-Zn-Pb VMS deposit with refractory Au signatures and low overall concentrations versus the Kilmacoo Au occurrence with visible phases of native Au and electrum with significant grades highlights the differing ore processes, and timing of emplacement. Late sulphide-bearing shear structures post-dating the formation of penetrative cleavages are now targets for structurally hosted Au mineralization.

Acknowledgments

We are grateful to Dr. Bill Sheppard and LiaMin Consulting for logistical support and access to archived samples. Access to drill core and the mine site was facilitated through IMC Exploration Group. This study was funded through a Geological Survey of Ireland Short Call Grant and with support from the Irish Centre for Research in Applied Geosciences, Science Foundation Ireland (SFI) (grant number 13/RC/2092) together with European Developments Funds and industry funding partners.

References

Chew DM & Stillman CJ (2009) Late Caledonian Orogeny and magmatism. In: The Geology of Ireland, 2nd edition, Dunedin Academic Press, Edinburgh, pp143-173.

McArdle P (1993) Evolution and preservation of volcanogenic sulphides at Avoca, southeast Ireland. Institute of Mining and Metallurgy Transactions Section B, 102:149-163.

McClenaghan SH, Lentz DR, Martin J & Diegor WG (2009) Gold in the Brunswick No. 12 volcanogenic massive sulfide deposit, Bathurst Mining Camp, Canada: evidence from bulk ore analysis and laser ablation ICP–MS data on sulfide phases. Mineralium Deposita, 44:523-557.

McClenaghan SH, Lentz DR & Cabri L (2004) Form of gold in massive sulfides: Textural evidence for the syngenetic deposition of gold in pyrite and arsenopyrite, Bathurst Mining Camp, New Brunswick. Canadian Mineralogist, 42:851-871.

McConnell BJ, Stillman CJ & Hertogen J (1999) An Ordovician basalt to peralkaline fractionation series from Avoca, Ireland. Journal of the Geological Society of London, 148:711-718.

Milner AL & McArdle P (1992) Gold mineralization in Ordovician volcanic rocks at Kilmacoo, Co. Wicklow: its exploration and geological controls. In The Irish Minerals Industry. Irish Association for Economic Geology, Dublin pp51-64.

Platt JW (1977) Volcanogenic mineralization at Avoca, Co. Wicklow, Ireland, and its regional implications. Geological Society of London, Special Publications, 7:163-170.

Sheppard WA (1980) The ores and host rock geology of the Avoca mines, Co. Wicklow, Ireland. Norges Geologiske Undersokelse, 360:269-283.

Stillman CJ & Williams CT (1979). Geochemistry and tectonic setting of some Upper Ordovician volcanic rocks in east and southeast Ireland. Earth and Planetary Science Letters, 42: 288-310.

Williams FM, Sheppard WA & McArdle P (1986) Avoca mine, County Wicklow: a review of geological and isotopic studies. In: Geology and Genesis of Mineral Deposits in Ireland. Irish Association for Economic Geology, Dublin, pp71-82.

Synvolcanic gold in the Archean – Recent contributions to genetic and exploration models, with examples from the Superior province, Canada

Patrick Mercier-Langevin and Benoît Dubé
Natural Resources Canada, Geological Survey of Canada

Abstract. Archean synvolcanic gold deposits represent desirable, but often challenging exploration targets. Such deposits primarily include gold-rich VMS, pyritic gold ±polymetallic vein and disseminated-style systems, and synvolcanic intrusion-hosted deposits.

The formation of Archean synvolcanic gold deposits can be the result of: 1) inherently Au-enriched source rocks and fluids due to a specific geodynamic setting or heritage and/or to a magmatic input, and, alternatively or additionally 2) efficient transport (favorable ligands) and precipitation (e.g. boiling/phase separation and zone refining).

Synvolcanic gold deposits are preferentially associated with transitional to calc-alkaline magmatic successions and andesite-dacite-rhyodacite-rhyolite magmatic suites comprising thick felsic units. Deposits formed in pericratonic settings, or on older crust basement in the early stages of rifting, are commonly slightly better endowed in gold than those formed in settings with no or limited basement influence. Evidence for a magmatic input include the presence of complex mineral assemblages (sulphosalts, sulphides, native elements, and tellurides), and anomalous trace element signatures (e.g. enrichment in the "epithermal suite" of elements Au-As-Sb-Ag-Hg and/or in felsic magma-associated elements Bi-W-Te-In-Sn). Large white mica±siliceous alteration, intense aluminous (variably metamorphosed argillic to advanced argillic-style) alteration, and heterogeneous Au distribution are also indicators of a possible magmatic contribution of Au, Ag, and other metals, such as Te and Bi.

1 Introduction

The Superior province is characterized by an exceptional gold endowment (>420 Moz Au, or 13,000 metric t: Dubé and Mercier-Langevin, *in prep*.) that is the result of a number of key factors that cumulated into forming a diversity of styles of mineralization through time and space. This is particularly the case in the different oceanic crust segments (greenstone belts) that are variably preserved in the southern part of the province (e.g., Abitibi belt). Although the bulk of the gold mineralization in the Superior formed over a relatively short period towards the end of the main north-south shortening episode (orogenic gold deposits), significant gold mineralization is synvolcanic. The synvolcanic gold mineralization therefore predates the peak of orogenic gold mineralization by a few tens of million years. However, the overlap in space with large orogenic gold deposits and districts and major synvolcanic gold deposits (e.g., southern Abitibi greenstone belt) is most likely related to common underlying causes (e.g., common source or recycling: Dubé et al. 2007b; Mercier-Langevin et al. 2014a), which may have implications on the understanding of ore-forming processes in the Archean.

2 Archean synvolcanic gold deposits

2.1 Deposits types and styles

Archean synvolcanic gold deposits are a subtype of Precambrian gold deposits formed early in the geological evolution of their host succession, i.e., prior to the onset of major regional compressional deformation. Synvolcanic gold deposits and prospects are present in both the Abitibi and Wabigoon subprovinces (Fig. 1) and show a large spectrum of sizes and styles.

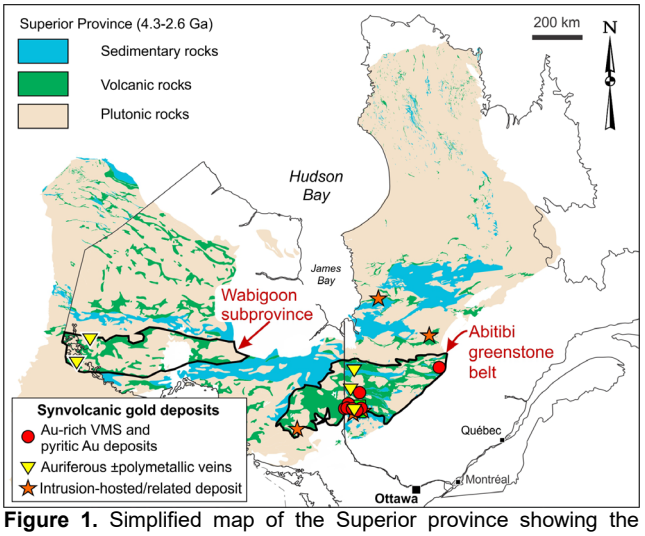

Figure 1. Simplified map of the Superior province showing the location of selected synvolcanic gold deposits.

Synvolcanic gold deposits can be hosted in volcanic ±sedimentary rocks and are associated with volcanism (Fig. 2), the most common types/styles being Au-rich volcanogenic massive sulphide (VMS) deposits, synvolcanic pyritic gold deposits, and auriferous ±polymetallic stockwork/disseminated sulphide systems (sometimes interpreted as epithermal-*like* deposits). They can also be hosted in intrusive rocks (Fig. 2) and associated with synvolcanic or pre-regional deformation intrusive bodies and generally consist of stockwork-disseminated-style sulphide zones (sometimes referred

to as porphyry-*like* or intrusion-related), and Au-Cu sulphide vein systems. A continuum between volcanic and intrusion-hosted deposits exists in many cases.

In many of the synvolcanic gold deposits, gold is a byproduct, except for a restricted number of deposits where it represents the principal, and in some cases, only commodity. Many of these deposits have been classified as gold-rich and auriferous VMS deposits based on anomalously high gold grades (e.g., ≥3.5 g/t Au) or a gold to base metal ratio greater than 1 (cf. Poulsen and Hannington 1996; Mercier-Langevin et al. 2011a). The gold-rich VMS-type deposits share broadly similar geometries, although each deposit presents some unique characteristics, whereas the pyritic gold, volcanic-hosted auriferous ±polymetallic veins and the intrusion-hosted deposits are all distinct.

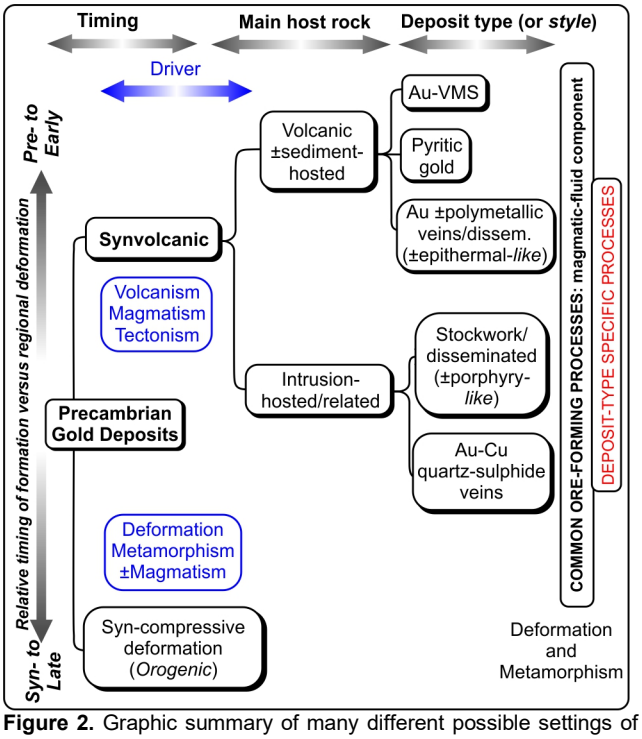

Figure 2. Graphic summary of many different possible settings of lode gold deposits highlighting synvolcanic gold deposits types, their drivers, and their settings. Modified from Dubé et al. (2015).

2.2 Timing of gold introduction

Synvolcanic gold deposits are formed during the volcanic-magmatic construction of their host sequence and in the vast majority of cases, the primary characteristics of such early styles of mineralization are obscured by overprinting deformation and metamorphism. Recent work has demonstrated that the syngenetic nature of many Archean gold deposits in the southern Superior province and research on active systems at sea made it clear that gold can be strongly enriched in volcanogenic submarine hydrothermal systems (Hannington et al. 2005, and references therein). However, establishing the precise timing of gold introduction in ancient systems can be difficult. Among the more robust indications of a synvolcanic timing for Au and associated alteration are: 1) overprint of structural fabrics and metamorphic minerals on the auriferous sulphides and associated alteration zones; 2) the presence of auriferous sulphide clast-bearing units associated with the ore in VMS environments; 3) spatial correlation between Au and the base metals at the scale of a deposit or lens; 4) spatial association of Au with synvolcanic/syngenetic alteration; 5) the presence of auriferous mineralization that is cut by synvolcanic (deformed) dykes; 6) stacking of auriferous sulphide zones in the volcanic sequence; and 7) gold-bearing late structural features devoid of Au when extending outside the limits of a sulphide orebody. The absence of isotopic (e.g., O, S, Pb) disturbance due to overprinting metasomatism associated with deformation and/or metamorphism is considered indirect evidence for syngenetic Au introduction, especially when supported by field evidence (Mercier-Langevin et al. 2015).

2.3 Ore-forming processes

Gold enrichment in synvolcanic gold deposits can be due to a series of specific features and processes active at different scales (Poulsen and Hannington 1996; Hannington et al. 1999; Huston 2000; Dubé et al. 2007a; Mercier-Langevin et al. 2011a, 2015).

Synvolcanic gold deposits can result from: 1) inherently enriched source rocks and deep-seated fluids, and/or 2) efficient transport (in aqueous fluid and/or vapour) and precipitation. These two conditions are not mutually exclusive, and different processes can be active at the same time and/or at the same site but at different scales (Fig. 3).

An inherently enriched source (magma or host sequence) and/or fluids, as suggested by the strong provinciality of synvolcanic gold deposits, and more particularly Au-rich VMS deposits (Fig. 1), can explain why some areas are so well endowed in synvolcanic gold. Enrichment in the source can be related to a specific geodynamic setting or heritage. It is commonly thought to be associated with a direct magmatic input of Au-bearing (and other metals) fluids into the ore-forming system (Fig. 3).

The geodynamic setting strongly influences not only the type of deposit (including synvolcanic examples) that is formed but also the metal budget. Mature submarine arc and arc – back-arc rift systems constructed on older crust appears to have influenced the overall Au budget of the deposits as indicated by their contaminated Pb-isotope signature and association with felsic rocks showing evidences of crustal contamination (e.g., inherited zircons, evolved Nd-isotope signature.

A preferential association of synvolcanic gold deposits with rifted arc and back-arc type settings, packages containing thick felsic volcanic rock and transitional to calc-alkaline andesite-dacite-rhyodacite-rhyolite magmatic affinities is another common characteristic of the synvolcanic gold deposit-bearing belts and districts (Mercier-Langevin et al. 2015 and references therein). Early rifting in an arc – back-arc-style environment is considered important in the genesis of the Au-rich VMS deposits of the Blake River Group in the southern Abitibi belt, where 6 of 11 of the richest and

largest Au-rich VMS deposits are located (Mercier-Langevin et al. 2011a, b). The concept of a favorable heritage or predisposition of certain areas of the upper mantle and lower crust to preconcentrate Au has been proposed for Phanerozoic belts where ore-forming processes tap the same enriched lithospheric mantle source for a prolonged period of time with the recurrent generation of Au deposits. This is perhaps related to favorable geodynamic conditions that fertilize the upper mantle and lower crust and link them to the upper crust (Sillitoe, 2008; Hronsky et al. 2012). Such favorable predisposition in the lower crust and/or upper mantle has been proposed to explain the strong provinciality of Au-rich VMS and orogenic Au deposits in the southern Abitibi belt (Dubé et al. 2007a; Mercier-Langevin et al. 2012). This uniquely endowed portion of the greenstone belt contains more than 85% the Au in the entire belt (all deposit types) and more than 90% of the synvolcanic Au (Mercier-Langevin et al. 2011a, 2014a).

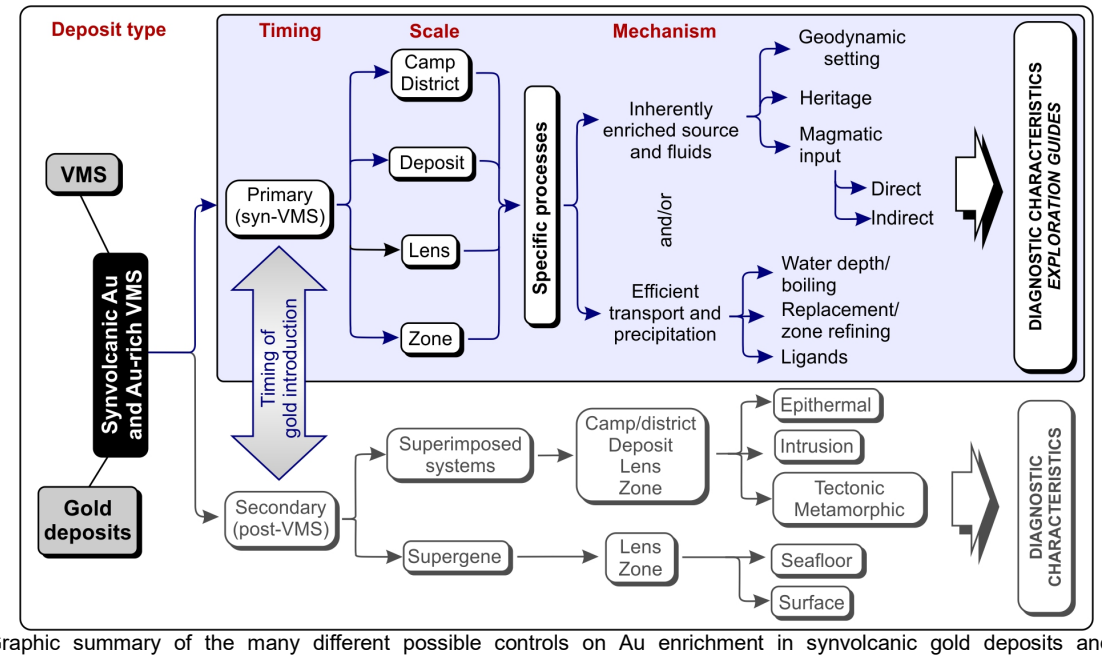

Figure 3. Graphic summary of the many different possible controls on Au enrichment in synvolcanic gold deposits and gold-rich volcanogenic massive sulphide deposits that operate on different spatial and temporal scales. From Mercier-Langevin et al. (2015).

A magmatic input of Au, either direct through degassing and/or fluid exsolution, or indirect through leaching of crystallized magma bodies at depth is a plausible mechanism to explain precious metal-enrichment in some synvolcanic gold deposits and districts as indicated by research on active systems and ancient deposits of the southern Superior. The evidence for a direct magmatic input of Au can be circumstantial, but the involvement of magmatic fluids can be readily inferred in many systems. The presence of extensive zones of aluminous alteration (metamorphosed advanced argillic alteration) has been interpreted as evidence for a magmatic input into the hydrothermal system (Dubé et al. 2007b; 2014; Mercier-Langevin et al. 2013, 2014b; Yergeau et al. 2015). Such aluminous alteration zones develop in response to H_2S vapour condensation or disproportionation of magmatically-derived SO_2 that produce very low-pH, acidic and oxidizing fluids that leach most elements in the rock except for Al and Si. Specific element suites, such as In, Te, and Bi in high-temperature Cu-rich ores and As, Sb, Hg, and Ag (the "epithermal suite") and complex sulphosalt assemblages in low-temperature Zn-rich ore also have been linked to a direct magmatic contribution of metals into the ore-forming hydrothermal system (Hannington et al. 1999; Huston et al. 2011).

Whereas some districts contain deposits that are uniformly enriched in Au, some districts/camps contain VMS deposits that are much more enriched than others in the same district (e,g, Horne and Quemont, Noranda district). This implies that local processes were involved in precious metal enrichment (i.e. efficient transport and precipitation mechanisms), including boiling/phase separation, optimal zone refining history, the availability of favorable ligands for transport, and the presence of elements acting as sinks for precious metals (e.g., Bi at Lemoine: Mercier-Langevin et al., 2014b). These processes control how gold is transported and deposited, and where in the system it may occur.

2.4 Ongoing research

Numerous synvolcanic gold deposits of the southern Superior appear to be associated with calc-alkaline intermediate to felsic centers that have unusually heavy whole-rock oxygen isotopic signatures, and most of these centers have been dated (U-Pb on zircon). The recovered zircons are currently being analyzed at the Geological Survey of Canada, the University of Alberta, and the University of Toronto for O, Li, and Hf isotopes, trace elements, and thermometry to better constrain the nature and evolution of the ore-associated magmas and

get a better understanding of the genesis of synvolcanic gold deposits at the Archean.

3 Conclusion

The classic exploration models used in Archean terranes for decades are being revised in part because there is clearly a much broader spectrum of gold deposit styles than previously considered. These include synvolcanic and synmagmatic ("syngenetic") deformed and metamorphosed gold deposits that are distinct from the orogenic model. Such a reappraisal has an impact on exploration models since significant gold mineralization formed during the volcanic construction of the greenstone belts. Evidence of the causative processes in Archean systems commonly is not observable in the field; therefore, exploration must focus on the visual evidence of the enrichment process(es) (or diagnostic features) that can be mapped at a range of different scales.

Large areas of the Archean cratons have not yet been explored thoroughly despite a great potential for precious and base metals, and more mature areas will have to be re-examined taking into account the potential for more diverse types of deposits than previously recognized.

Acknowledgements

Sincere thanks to numerous colleagues from the federal and provincial surveys, academia, and the industry, and more particularly to numerous students, for sharing their knowledge of Archean gold deposits, and for access to study sites and material.

References

Dubé B, Mercier-Langevin P (*in prep*) Gold deposits of the Abitibi greenstone belt. Econ Geol.

Dubé B, Gosselin P, Mercier-Langevin P, Hannington M Galley A (2007a) Gold-rich volcanogenic massive sulphide deposits. Geological Association of Canada, Mineral Deposits Division Special Publication 5:75–94.

Dubé B, Mercier-Langevin P, Hannington M, Lafrance B, Gosselin G, Gosselin P. (2007b) The LaRonde Penna world-class Au-rich volcanogenic massive sulfide deposit, Abitibi, Québec: Mineralogy and geochemistry of alteration and implications for genesis and exploration. Econ Geol 102:633-666.

Dubé B, Mercier-Langevin P, Kjarsgaard I, Hannington M, Bécu V, Côté J, Moorhead J, Legault M, Bédard N (2014) The Bousquet 2-Dumagami world-class Archean Au-rich volcanogenic massive sulfide deposit, Abitibi, Quebec: Metamorphosed submarine advanced argillic alteration footprint and genesis. Econ Geol 109:121-166.

Hannington MD, Poulsen KH, Thompson JFH, Sillitoe RH (1999) Volcanogenic gold in the massive sulfide environment. In: Barrie CT, Hannington MD (eds) Volcanic-associated massive sulfide deposits: processes and examples in modern and ancient settings. Reviews in Economic Geology 8. Society of Economic Geologists, Littleton, pp 325–356.

Hannington MD, de Ronde CEJ, Petersen S (2005) Sea-floor tectonics and submarine hydrothermal systems: Economic Geology 100th Anniversary Volume, pp 111-141.

Hronsky JMA, Groves DI, Loucks RL, Begg GC (2012) A unified model for gold mineralisation in accretionary orogens and implications for regional-scale exploration targeting methods. Mineral Deposita 47:339-358.

Huston DL (2000) Gold in volcanic-hosted massive sulfide deposits: Distribution, genesis, and exploration. In: Hagemann SG, Brown PE (eds) Gold in 2000. Reviews in Economic Geology 13. Society of Economic Geologists, Littleton, pp 400-426.

Huston DL, Relvas JMRS, Gemmell JB, Drieberg S (2011) The role of granites in volcanogenic massive sulfide deposits. Mineral Deposita 46:473-507.

Mercier-Langevin P, Hannington MD, Dubé B, Bécu V (2011a) The gold content of volcanogenic massive sulfide deposits. Mineral Deposita 46:509-539.

Mercier-Langevin P, Hannington M, Dubé B, McNicoll V, Goutier J, Monecke T (2011b) Geodynamic influences on the genesis of Archean world-class gold-rich VMS deposits: examples from the Blake River Group, Abitibi Grenstone Belt, Canada. Procedings of the Eleventh Biennial SGA Meeting, Antofagasta, Chile, Volume 1:85-87

Mercier-Langevin P, Houlé MG, Dubé B, Monecke T, Hannington MD, Gibson HL, Goutier J (2012) A special issue on Archean magmatism, volcanism and ore deposits: Part 1. Komatiite-associated Ni-Cu-(PGE) sulfide and greenstone-hosted Au deposits – Preface. Econ Geol 107:745-753.

Mercier-Langevin P, McNicoll V, Allen RL, Blight JHS Dubé B (2013) The Boliden gold-rich volcanogenic massive sulfide deposit, Skellefte district, Sweden: new U-Pb age constraints and implications at deposit and district scale. Mineral Deposita 48:485-504

Mercier-Langevin P, Gibson HL, Hannington MD, Goutier J, Monecke T, Dubé B, Houlé MG (2014a) A special issue on Archean magmatism, volcanism and ore deposits: Part 2. Volcanogenic massive sulfide deposits – Preface. Econ Geol 109:1-9.

Mercier-Langevin P, Lafrance B, Bécu V, Dubé B, Kjarsgaard I, Guha J (2014b) The Lemoine auriferous volcanogenic massive sulfide deposit, Chibougamau camp, Abitibi greenstone belt, Quebec: Geology and genesis. Econ Geol 109:231-269.

Mercier-Langevin P, Hannington MD, Dubé B, Piercey SJ, Peter JM, Pehrsson SJ (2015) Precious metal enrichment processes in volcanogenic massive sulphide deposits – a summary of key features, with an emphasis on TGI-4 research contributions: Geological Survey of Canada Open File 7853:117-130.

Poulsen KH, Hannington MD (1996) Volcanic-associated massive sulphide gold. In: Eckstrand OR, Sinclair WD, Thorpe RI (eds) Geology of Canadian mineral deposit types: Geology of Canada 8:183-196.

Sillitoe RH (2008) Major gold deposits and belts of the North and South American Cordillera: Distribution, tectonomagmatic settings, and metallogenic considerations. Econ Geol 103:663-687.

Yergeau D, Mercier-Langevin P, Dubé B, Malo M, McNicoll VJ, Jackson SE, Savoie A, La Rochelle F (2015) The Archean Westwood Au deposit, southern Abitibi: Telescoped Au-rich VMS and intrusion-related systems: Geological Survey of Canada Open File 7852:177-191.

Fluid constraints for Au deposition at the *Monges* iron deposit, Ossa-Morena Zone (Montemor-o-Novo, Portugal)

Maia Miguel, São Pedro Diogo, Nogueira Pedro
School of Sciences and Technology of the University of Évora; Institute of Earth Sciences

Mirão José
School of Sciences and Technology of the University of Évora; HERCULES Laboratory of the University of Évora

Noronha Fernando
Faculty of Sciences of the University of Porto; Institute of Earth Sciences

Abstract. The Monges deposit was an important iron mine during late 19th and early 20th century. In recent decades the region of Montemor-o-Novo has attracted the interest of several exploration companies due to high-grade gold anomalies found through soil geochemistry work. Exploration drilling carried out in the WNW-ESE and conjugated N-S shear-zones (≈30 km) identified interesting gold grades, including in the vicinity of the Monges iron deposit. The fluid inclusion study presented here is focused on constraining the fluids related to iron and gold mineralization processes. Fluid constraints for the iron mineralization are difficult assess in the early stage (SEDEX environment) of the Ossa-Morena Zone geodynamic evolution. An overprinting of these early fluids is found, and most of the fluids present may be related to late metamorphism. Gold in Monges area shows affinity to a H_2O-CO_2-NaCl fluid system showing evidence of immiscibility and trace concentrations of CH_4. The geological settings hosting gold mineralization as well as the fluid characteristics with low-salinity, with an average of 7.72 wt. % NaCl Equiv. and homogenization temperatures between 150ºC and 350ºC, points towards an orogenic gold deposit model, corroborating and reinforcing the current accepted model for gold mineralization of Montemor-o-Novo region.

1 Introduction

The Ossa-Morena Zone (OMZ, Portugal) comprises a Fe-Zn metallogenic belt (Montemor-Ficalho) that hosts several Fe deposits with different recognized metallogenic origins, such as, 1) Fe-Skarn deposits related with Variscan igneous intrusions (Orada, Azenhas and Alvito deposits); and 2) massive iron ore deposits hosted in carbonate and calcsilicate rocks that are currently accepted to have formed in a SEDEX-VMS continuum which is the case of Montemor-o-Novo ancient mining complex (Salgueiro 2011, Salgueiro et al. 2011). Monges is part of the Montemor-o-Novo area composed of 10 iron ore mining sites and was the largest mine regarding its size and tonnage of iron ore exploited. The ore is mainly magnetite and the ore paragenesis is magnetite + pyrite + hematite + pyrrhotite (± chalcopyrite).

These mines ceased all exploitation in early 20th century, more recently, gold anomalies were found through soil geochemistry, attracting exploration companies to the area. These companies carried out prospecting that revealed new data and interesting gold grades along a WNW-ESE shear zone (Montemor-o-Novo shear) which inflects to a N-S direction in the southeastern part of the shear belt (Ribeiro et al. 1993). This work aims to characterize the gold mineralization and its relationship with iron ore deposits that are spatially associated. Seven boreholes from the Monges area were sampled to characterize the fluids involved in the mineralization genesis; for this study samples from two boreholes were selected.

2 Geological setting

The Serra do Monfurado, where the Monges area is located, is characterized by three main geological formations (Araújo 1995; Chichorro 2006).

i) Escoural Formation (Ediacarian to Lower Cambrian) – characterized by black-schists with sparse intercalation of felsic rocks.

ii) Monfurado Formation (Lower-Middle Cambrian) – a lower unit composed of felsic magmatic rocks (leptinites), and an upper unit of calcsilicate (skarn-like) rocks, marbles and dolomitic limestones;

iii) Carvalhal Formation (Middle-Upper Cambrian) – mainly characterized by banded and massive amphibolites with N-MORB and E-MORB signatures.

2.1 Iron-oxide mineralization

In the Monges mine magnetite occurs as a massive ore (stratiform) and as disseminated mineralization in chloritic-amphibolitic marbles and calcsilicate rocks (skarn-like) from the Monfurado Formation (Salgueiro 2011 and references therein). Remobilization and reprecipitation has resulted in late cross-cutting vein structures and a magnetite + barite primary assemblage is commonly found in waste rock disposals.

2.2 Gold mineralization

Gold mineralization from Montemor-o-Novo developed within a late-Variscan WNW-ESE shear-zone, along a 30km belt which inflects to N-S direction in its most SE

zone, close to the Boa-Fé village (Ribeiro et al. 1993, Chichorro 2006, Inverno 2011). Gold mineralization is usually hosted in shear-zones affecting the Carvalhal and Escoural Formations, where higher gold grades are found.

The main identified gold-bearing mineral assemblages are arsenopyrite, loellingite and pyrite, although hedleyite, native bismuth and maldonite were also found associated with quartz and calcite (São Pedro 2019, in prep.). These mineral assemblages are typically accompanied by intense hydrothermal alteration, such as sericitization and intense chloritization (propylitic alteration).

3 Fluid inclusions study

For this study eleven doubly polished thick sections were prepared (≈200 µm). Sampling was mainly focused in quartz (+ calcite) veins cross-cutting the host rocks. Over 300 individual fluid inclusions were studied using a LINKAM THMSG 600 microthermometry stage attached to a Nikon Eclipse 50Ipol with 100x long focus objective lens.

3.1 Fluid inclusion petrography

Fluid inclusions hosted in quartz, hornblende, tremolite and barite crystals were studied. Hornblende and tremolite were identified in late veins and in matrix alteration in felsic metavolcanic and calcsilicate (skarn-like) rocks from the Monfurado Formation. These minerals are interpreted to have formed during late metasomatic alteration of the host rocks in the shear zone.

Fluid inclusion petrography revealed two main FI types throughout all the studied samples, defined as Type I and Type II (Fig. 1 A-B).

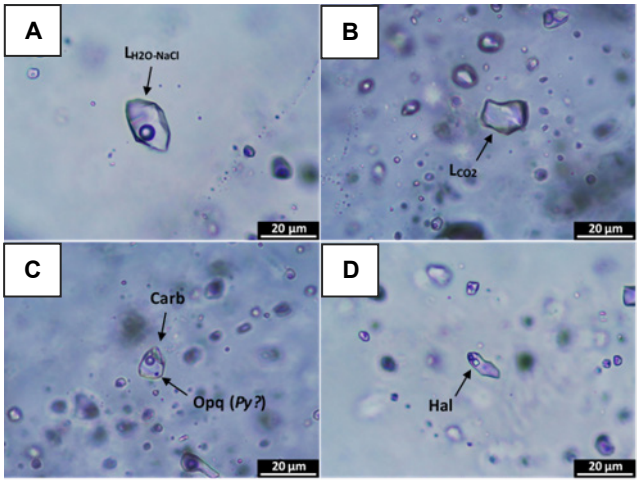

Figure 1. Examples of FI types from Monges samples where: **a.** Type I FI; **b.** Type II FI; **c.** Multisolid FI with an opaque (opq) and carbonate (carb) daughter mineral; **d.** Type I Halite-bearing FI.

Type I consists of two-phase fluid inclusions containing H_2O liquid and vapor phases. These FI show predominantly negative crystal shapes when related to primary fluid inclusion assemblages (FIA) and irregular shapes in secondary FIA´s, although this is not a necessary distinguishing factor between the two FIA´s. Three phase NaCl oversaturated FIs were rarely identified in the studied samples, and are grouped in this type, containing H_2O liquid-rich and vapor phases and a halite crystal at room temperature (≥25ºC) (Fig. 1-D).

Type II fluid inclusions are characterized by two and three-phase FI´s and were subdivided as Type II.a and Type II.b respectively. Type II.a FIs are multiphase having a CO_2-rich liquid phase plus an aqueous liquid phase. A CO_2 vapor phase may sometimes be present at temperature of 25ºC. Type II.b consists of two phase insluions with a CO_2-liquid phase and a CO_2 vapor phase.

Although these FI types are clearly predominant in the studied samples, it is important to note that CH_4 liquid-rich fluid inclusions occur with Type II FI cluster assemblages. Several inclusions from Type I and Type II were identified as containing one or two solid phases in their composition, sometimes with an opaque daughter mineral (Fig. 1.C).

3.2 Microthermometry data

Figure 2 plots Salinity (wt. % NaCl Equiv.) versus Th, displaying the microthermometry results of all the FI's studied, arranged by host mineral.

Type I FI´s eutectic temperatures (T_e) range between -10.2ºC and -49.4ºC, corresponding to fluids with several solutes in its composition, such as, NaCl, MgCl and $CaCl_2$. Salinities were calculated from ice melting temperatures (Tm_{ice}), ranging from 0.88 and 23.18 wt. % NaCl Equiv. with a mean of 7.72. Homogenization temperatures (T_h) were measured between 116ºC and 460ºC, with a T_h average of 253ºC. There were decrepitation temperatures (T_d) measured between 216ºC and 247ºC. Type I FI data includes the FI´s where one or two daughter mineral phases were found, with higher salinities - ranging from 32.9 to 34.7 wt. % NaCl Equiv. (calculated from halite melting temperature, Tm_{Hal}) and T_h values of 116ºC, where vapor homogenized into liquid and Th < Tm_{Hal}.

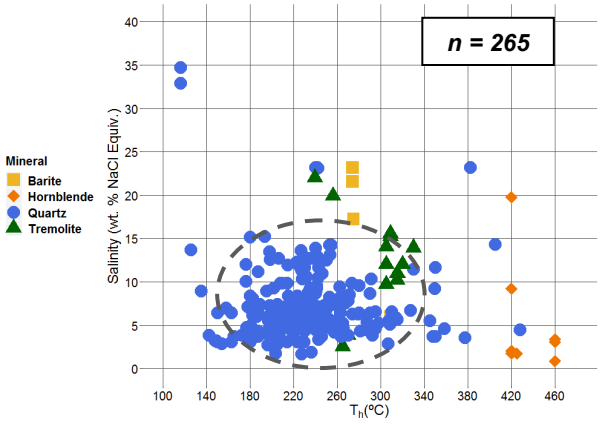

Figure 2. Salinity (wt. % NaCl Equiv.) versus Th, for Type I FI, organized by host mineral. The dashed line represents 95% of the data.

Type II FIs were studied exclusively in quartz crystals and subdivided into Type II.a and Type II.b due to their different compositions. Type II.a FIs revealed CO_2 melting temperatures (Tm_{CO2}) ranging from -58.6ºC and -56.8ºC, with corresponding CO_2 homogenizations (Th_{CO2}) between +3.9ºC and +24.6ºC. Salinities range from 7.17 and 18.04 wt. % NaCl Equiv.

Type II.b shows liquid CO2 as their dominant component, and Tm_{CO2} range from -57.5ºC and -56.8ºC. Th_{CO2} were measured from 0ºC and 5ºC.

3.3 Raman spectroscopy

Raman spectroscopy was carried out on the main FI types aiming to identify the volatiles and solids observed in FIs during petrography and microthermometry studies.

Figure 3-A shows a barite typical Raman spectrum with its characteristic main Raman vibrations at 986 cm^{-1} (v1), 458 cm^{-1} (v2), 1141 cm^{-1} (v3), 615 cm^{-1} (v4), which allowed for the identification of the host mineral of some of the studied FIs.

The solids present in Type I FIs were studied by this technique allowing the identification of calcite as the main daughter mineral phase (1084 cm^{-1}) (Figure 3-B). The opaque daughter mineral found in some FI's could not be identified due to its small size (≈ 1 µm).

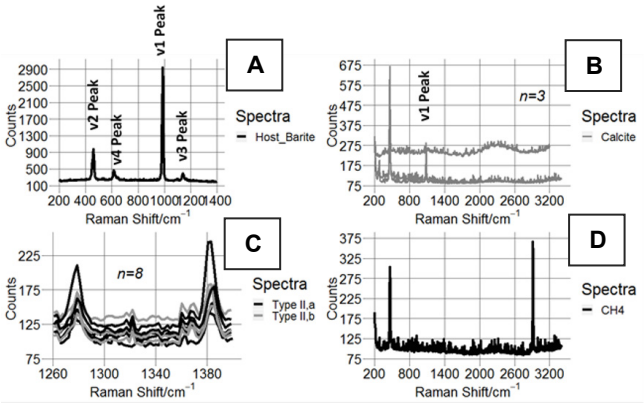

Figure 3. Collected Raman spectra for FIs. **a**. Barite host mineral. **b.** Calcite identification with main Raman vibration of 1084 cm^{-1}. **c.** Raman spectrum from liquid CO_2 analysis of Type II subtypes. **d.** Raman spectrum example of liquid CH_4.

Liquid CO_2 was identified in Type II (Type II.a and Type II.b) FIs by its characteristic Raman main vibrations of 1285 cm^{-1} and 1388 cm^{-1} (Fermi doublet). The obtained spectra allow for the calculation of the Fermi Diad distance (Δ), in order to determine the CO_2 density (g/cm^3) for these types of FIs. Figure 3-C shows some of the obtained spectra for Type II.a and Type II.b FIs. Fermi Diad distance of Type II.a range from 104.25Δ and 107.22Δ with an average of 105.75 Δ corresponding to a CO_2 density of 1.2 g/cm^3. Type II.b FIs showed Fermi Diad distances between 104.25 and 106.52Δ with an average of 105.00Δ, which corresponds to CO_2 densities of 0.92 g/cm^3. The average values between these two subtypes of Type II FI´s reveal a 105.38Δ distance indicating a CO_2 density of 1.06 g/cm^3. Although their scarcity, several CH_4-bearing fluid inclusions were identified and studied, Raman spectroscopy shows that these FI´s composition is near a pure CH_4 composition (Fig. 3-D).

4 Fluid flow contribution for mineralization

The gathered FI data reflects the fluid circulation in the Montemor-o-Novo shear zone affecting the Escoural, Monfurado and Carvalhal Formations, where gold-mineralization occurs. This puts aside the possibility that the studied fluids are related to the iron mineralization of the Monges deposit, which precedes the gold-related mineralizing events. Primary fluids were most certainly overprinted by late-metamorphic fluids as can be evidenced by the FI present in the amphibole group minerals. Therefore, the data gathered in this study concerns mainly the late episodes related to the gold ore genesis. This study provides evidence for a revised metallogenic model for gold emplacement for the Ossa-Morena Zone.

Previous studies classify the Montemor-o-Novo deposit as an orogenic gold related deposit (Ribeiro et al. 1993, Pereira et al. 2002, Inverno, 2011). The metallogenic models have been supported by regional structural studies and hydrothermal alteration geochemistry, although, no fluid inclusion studies were ever carried out. The work presented herein is the first FI study elucidating gold transport and deposition in the Montemor-o-Novo gold deposit.

The iron and gold mineralizations although being in the proximity of one another, clearly show different genetic and metallogenic evolutions.

4.1 New Research

The relatively low salinity fluids (< 10 wt. % NaCl Equiv.) and T_h temperatures between 150ºC and 350ºC are consistent with typical fluid properties identified for orogenic gold deposits worldwide (Bodnar et al. 2014).

The T_e (first ice melting temperatures) range indicates the presence of Mg^{2+} and Ca^{2+} in the fluids trapped in Type I FIs (Fig. 4). The presence of these ions justifies the crystallization of calcite daughter minerals in some of the studied FIs.

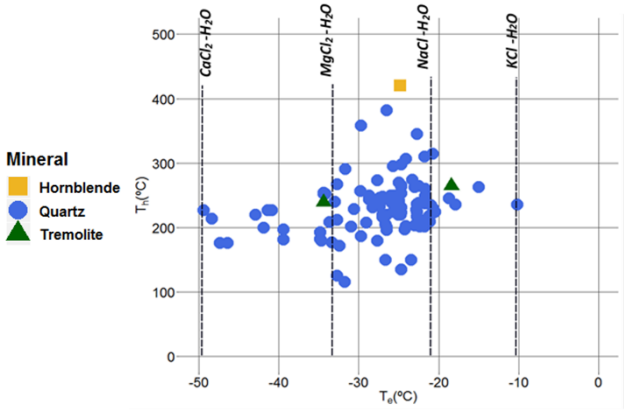

Figure 4. Th versus Te plot showing the solutes content in the different types of FI´s. Content estimated from first ice melting temperatures.

The higher T_h values found in Type I FIs were recorded in metamorphic amphiboles (hornblende and tremolite) indicating that metamorphic fluids reached temperatures of 460ºC, close to metamorphic peak conditions described for the region (Pereira et al. 2012).

Type II CO_2-bearing fluid inclusions in assemblages with Type I FI´s indicated a H_2O-CO_2-NaCl system. The different H_2O and CO_2 concentrations suggest that immiscibility occurred, reflecting devolatilization of the amphibolite and black-schist units. Halite bearing fluid inclusions are rare (two FI´s registered) and are not representative of the mineralizing fluids (Robert et al 1995; Boullier et al. 1998).

CH_4 concentrations in H_2O-CO_2-NaCl and CO_2-pure FIs is estimated to be ≈ 5 mol. % (Fig. 5). Nevertheless, liquid CH_4 bearing FIs were found in samples from quartz veins that cross-cut carbonate/calcsilicate host rocks and could be evidence of organic matter thermal degradation in these lithologies (Demir et al. 2017).

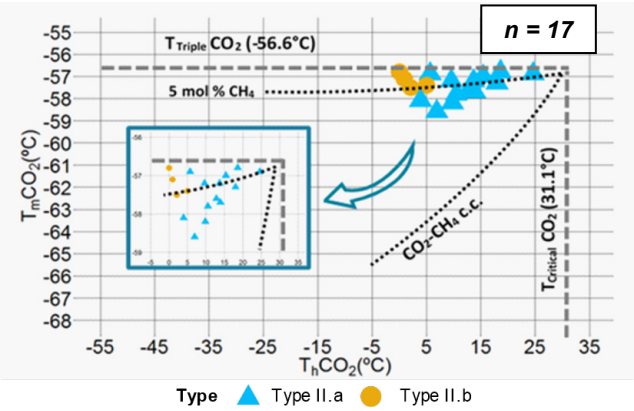

Figure 5. Tm_{CO2} versus Th_{CO2} plot from CO_2-bearing fluid inclusions. Trend lines adapted from Bodnar et al. (2014).

5 Conclusions

Data suggests that gold mineralization originated from low to medium salinity fluids in a H_2O-CO_2-NaCl system, containing variable concentrations of CO_2 in their composition. This indicates that immiscibility occurred, possibly due to fluid pressure cycles promoted by cyclical reactivation of the host shear zones in ductile and brittle regimes (Ribeiro et al. 1993). Fluid temperatures ranged from 150ºC to 350ºC, although during peak metamorphism they could be higher than 460ºC, as seen in FIs hosted by amphibole.

The data corroborates the orogenic gold model accepted for this deposit, although, identifying a clear source for the gold-bearing fluids is unresolved. The data presented here closely approaches a model where fluids may have had a high metamorphic devolatilization contribution generated by the Montemor-o-Novo WNW-ESE and N-S Boa-Fé shears.

Acknowledgements

The authors thank the HERCULES Laboratory of the University of Évora for Raman Spectroscopy equipment usage. This work is a contribution to the project "ZOM-3D Metallogenic Modelling of Ossa-Morena Zone: Valorization of the Alentejo Mineral Resources" (ALT20-03-0145-FEDER-000028), funded by Alentejo 2020 (Regional Operational Program of Alentejo) through the FEDER / FSE / FEEI. M. Maia, D. São Pedro, F. Noronha and P. Nogueira acknowledge the funding provided by the Institute of Earth Sciences (ICT), under contract with FCT (UID/GEO/04683/2013) and to COMPETE POCI-01-0145-FEDER-007690.

References

Araújo A, Ribeiro A (1995) Tangential Transpressive Strain Regime in the Évora – Aracena Domain (Ossa Morena Zone). Boletín Geol. y Min., 106:111-117.

Bodnar RJ, Lecumberri-Sanchez P, Moncada D, Steele-McInnis, M (2014) Fluid Inclusions in Hydrothermal Ore Deposits. Treatise on Geochemistry, 2nd Edition, Chapter: 13.5.

Boullier A-M, Firdaous K, Robert F (1998) On the significance of aqueous fluid inclusions in gold-bearing quartz vein deposits from the southeastern Abitibi Subprovince (Quebec, Canada). Econ. Geol. 93:216–223.

Chichorro M (2006) A evolução tectónica da zona de cisalhamento de Montemor-o-Novo (Sudoeste da Zona de Ossa Morena – Área de Santiago do Escoural – Cabrela). PhD Thesis, Univ. Évora, Évora.

Frezzotti ML, Tecce F, Casagli A (2012) Raman Spectrosocopy for fluid inclusion analysis. J Geochem Explor, 112:1-20.

Demir Y, Uysal I, Kandemir R, Jauss A (2017) Geochemistry, fluid inclusion and stable isotope constraints (C and O) of the Sivrikaya Fe-skarn mineralization (Rize, NE Turkey). Ore Geol. Rev, 91:153-172.

Inverno CMC (2011) Comparação entre os jazigos de ouro do tipo orogénico (ou mesotermais) e os jazigos de ouro associados a intrusão. Algumas extrapolações para Portugal. Cadernos Lab. Xeol. Laxe, 36:99-156.

Pereira MF, Silva JB, Chichorro M (2002) Field guide to Cadomia-2002 Workshop – The Cadomian basement of the Ossa-Morena Zone (Iberian Massif) in Northeast and West Alentejo, Portugal, Univ. Évora, 50 p.

Pereira MF, Chichorro M, Brandão Silva J, Ordóñez-Casaso B, Lee JKW, Williams IS (2012) Early carboniferous wrenching, exhumation of high-grade metamorphic rocks and basin instability in SW Iberia: Constraints derived from structural geology and U–Pb and 40Ar–39Ar geochronology. Tectonophysics.

Ribeiro A, Mateus A, Barriga F (1993) Gold mineralizations of the Escoural area (Montemor-o-Novo, Évora, Portugal): A progress report. Comun. XII Reun. Geol. Oeste Penins., 1:215-226.

Robert F, Boullier A-M, Firdaous K (1995) Gold-quartz veins in metamorphic terranes and their bearing on the role of fluids in faulting. J. of Geophys. Res. 100:12–12,879.

Salgueiro R (2011) Caracterização e génese das mineralizações de magnetite – sulfuretos em Monges (Santiago do Escoural, Montemor-o-Novo) e ensaio comparativo com as suas congéneres em Orada-Vale de Pães (Serpa-Vidigueira). Tese de Doutoramento, Univ. Lisboa, 524 p.

Salgueiro R, Inverno C, Mateus A, (2012) Mineralizações de Magnetite e Sulfuretos de Monges (Santiago do Escoural, Montemor-o-Novo), Vale de Pães (Cuba-Vidigueira) e Orada (Pedrógão, Serpa): Síntese de ensaio comparativo. Boletim de Minas, 47 (1).

São Pedro D (2019, *in prep.*) Estudo mineralógico e geoquímico do depósito Aurífero de Casas Novas (*Montemor-o-Novo, Portugal*). Master´s Thesis, Faculty of Sciences of Univ. Évora, Évora.

The presence of colloidal gold in epithermal mineralizing fluids

Gülcan Bozkaya
Pamukkale University, Department of Geological Engineering, Turkey

David A. Banks
School of Earth and Environment, University of Leeds, U.K.

Ömer Bozkaya
Pamukkale University, Department of Geological Engineering, Turkey

Abstract. Transport of gold and silver as colloidal particles has been observed in c. 300 ^{O}C low salinity fluids from the Arapucandere intermediate sulphidation epithermal base-metal-Au deposit in NW Turkey. Large euhedral quartz crystals, grew after the deposition of sulfides. Overgrowths have a fibrous texture which grew perpendicular to the existing crystal faces and facilitated trapping of large elongate fluid inclusions between the quartz fibres. Episodic trapping of fluid inclusions occurred throughout the growth of quartz. Trapped within primary fluid inclusions are numerous particles of gold, the largest observed is c. 1 μm but most are smaller. BSE element mapping show these to contain Au, Ag, Cu + Hg. LA-ICP-MS ablation of fluid inclusions confirms Au and Ag is not present in solution, occurring as numerous particles. The concentration of gold in fluid inclusions is orders of magnitude greater than has been previously measured or thought likely in crustal fluids. The average Ag concentration is c. 32 ppm and Au is c. 41 ppm, but the maximum concentrations may reach several 100's to 1000 ppm. Au-Ag particles could not have precipitated in the fluid inclusions, therefore have precipitated elsewhere and transported by the hydrothermal fluid.

1 Introduction

Concentrations of gold are usually very low and difficult to determine in fluid inclusions, which are micron sized aliquots of the mineralizing fluid trapped in minerals that precipitated during mineralization. The inability to measure gold concentrations was a fundamental problem in understanding key processes that transport and precipitate the metal. Recent technological advances now allow direct measurement of Au concentrations in the ore-forming fluids trapped in various minerals as fluid inclusions. This study provides evidence for the presence of colloidal Au-Ag particles in epithermal fluids through their observation, using scanning electron microscopy (SEM), in primary fluid inclusions trapped during the different stages of growth of large quartz crystals. SEM cathodoluminescence (SEM-CL) was used to define the multiple growth stages of the quartz which were linked to different generations of largely primary fluid inclusions, which record rapid changes in pressure and temperature. Microthermometry of the fluid inclusions constrained pressure, temperature and salinity of the hydrothermal fluids over the period of euhedral quartz growth. Combining the salinity of the fluid inclusions with laser ablation-inductively coupled plasma- mass spectrometry (LA-ICP-MS) of individual fluid inclusions allowed the concentration of Au and Ag to be determined and in what form Au and Ag were present.

2 Geological setting

The Arapucandere deposit can be considered as an intermediate-sulfidation epithermal deposit hosted by Palaeozoic metamorphic rocks and Permo-Triassic clastic rocks related to the collisional and post-collisional tectonic regime in the Biga Peninsula. Mineralization at Arapucandere, which was a base-metal deposit, results from episodic lithostatic–hydrostatic pressure variations (Bozkaya and Banks 2015) within fault and fracture systems creating space for mineralization and providing a mechanism that induces massive ore deposition. Quartz is present as largely pre-ore coarse crystals and syn-to post ore finer-grained crystals. Different episodes of deposition for each type of quartz are evident indicating repeated influx of fluids. Sulfides, sphalerite, galena and chalcopyrite, cut the coarser grained quartz and also show evidence of multiple periods of deposition. Pyrite is an early phase, occurring within the quartz that is cut by other sulfides.

3 Fluid Inclusion analyses

Primary inclusions are located in zones where, predominantly L-V, fluid inclusions are trapped in significant numbers in linear arrays originating from existing crystal faces (Fig. 1). These are typically between 20 μm and 100 μm in size (Fig. 2). V-rich inclusions are much less common, but may occur with L-V inclusions in these linear trails. V-rich inclusions frequently occur in fractures that appear to be pseudo-secondary where trails originate from the outer surface of the quartz crystal, however they may also be of secondary origin. There are also examples of clear secondary fluid inclusions as seen in CL where a trail of inclusions starts in the later quartz growth and cuts the

outer face of the euhedral crystal and through numerous growth bands.

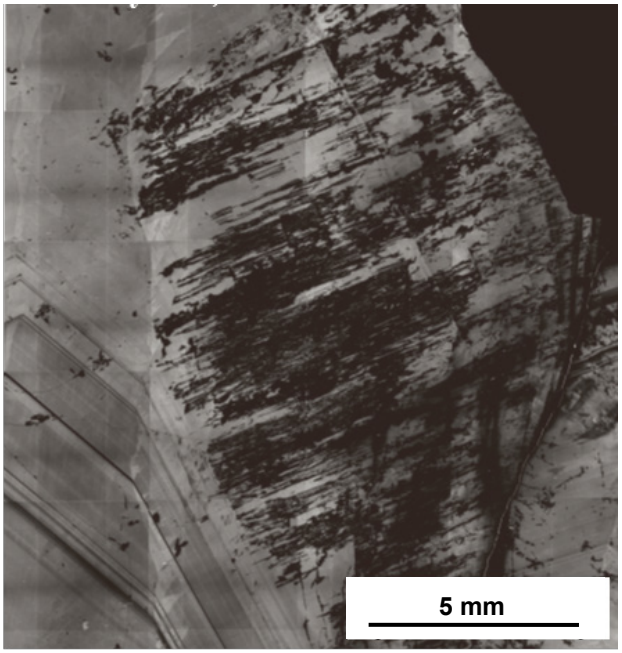

Figure 1. SEM-CL images of growth textures relative to Primary L-V, V-L fluid inclusions. Dark areas are long elongate trails of fluid inclusions originating at distinct crystal growth faces.

Th values are between 270 and 340 ^{O}C and the majority of the salinities are low c. < 2 wt.% NaCl equiv. but a small number of areas, where the inclusions appear to secondary, have salinities up to c. 8 wt.% NaCl equiv.

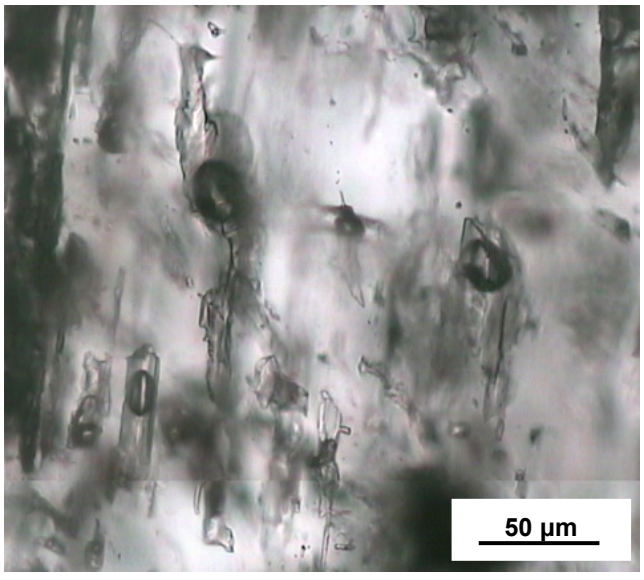

Figure 2. Trails of elongate inclusions trapped between fibrous quartz. These inclusions are the dark areas in Figure 1.

Although V-rich inclusions can be large > 30 µm, the small amount of liquid made determination of their salinity difficult. They do exist in inclusion clusters together with what appear to be V-only inclusions and inclusions with variable L/V ratios (Fig. 2). Overall the measured T_h values of V-rich inclusions (homogenize to vapor) are consistent with the T_h values of L-V inclusions that (homogenize to liquid) and so in some of the zones homogenization to both liquid and vapour occurs, indicating there was boiling.

4 SEM observations

Due to their large size many fluid inclusions were opened during polishing of wafers which were used both for fluid inclusions and CL. In the CL images, bright mineral/solid inclusions were observed in open fluid inclusions. Two open inclusions of c. 50 µm size are shown in the back scattered electron (BSE) image Figure 3a.

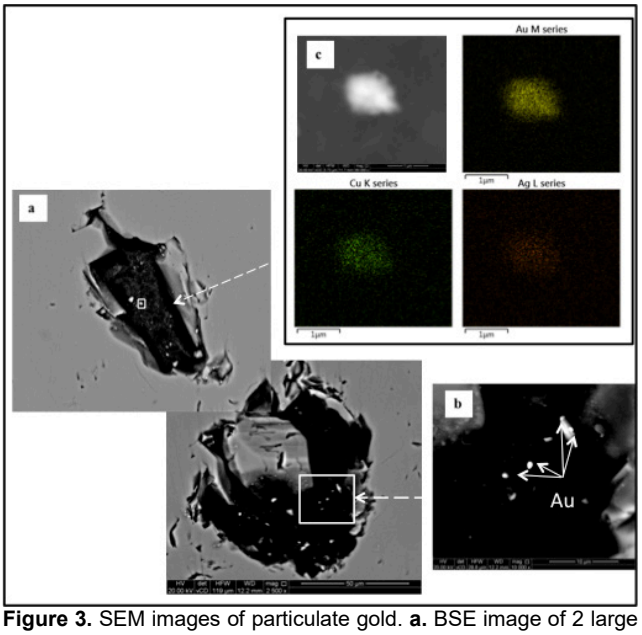

Figure 3. SEM images of particulate gold. **a.** BSE image of 2 large opened fluid inclusions, from the area in b, showing bright spots corresponding to Au, with Ba, Pb and Fe also present. **b.** Magnified area with a number of gold particles as the brightest rounded grains. **c.** BSE element mapping of the largest c.1.5 µm particle and element maps for Au, Ag and Cu.

In both inclusions and in almost all open inclusions imaged by BSE, several sub-micron gold particles can be seen (Fig. 3b) with the largest being c. 1 µm in size, but they are commonly smaller than this. These are attached to the walls of the inclusion or on calcite or baryte crystals. Gold particles can be distinguished as they are always rounded and are the brightest objects, for example (Fig. 3c) where the two brightest inclusions are attached to a more rectangular, less bright, baryte. With the largest gold inclusions, it was possible to use BSE element mapping to obtain compositional data that showed there was silver, copper and occasionally mercury in addition to gold (Fig. 3c). Other small crystals are present in the inclusions and energy dispersive spectroscopy (EDS) identified these as pyrite, baryte, galena, sphalerite and calcite (spectra are presented in supplementary data). Element mapping of the fluid inclusions content (Fig. 4) shows the presence of small

individual mineral crystals and also that the inner surfaces are coated in calcite and sulphides/sulphates.

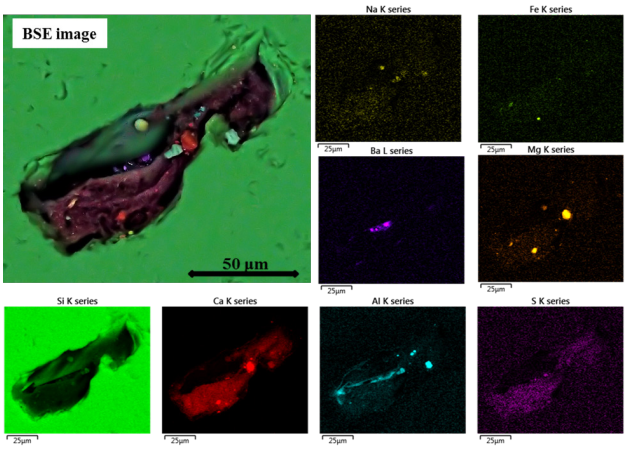

Figure 4. Composite element map of a large open fluid inclusion and individual element distributions. Ca and S coat a large proportion of the inclusion. Individual crystals of other elements are present.

The actual number of gold particles and other minerals in the fluid inclusions is unclear as an unknown number would have been lost when the inclusions were opened during polishing. At greater magnification (Fig. 5) the BSE image of part of the inner surface of the inclusions in figure 4 shows numerous sub-micron gold particles,

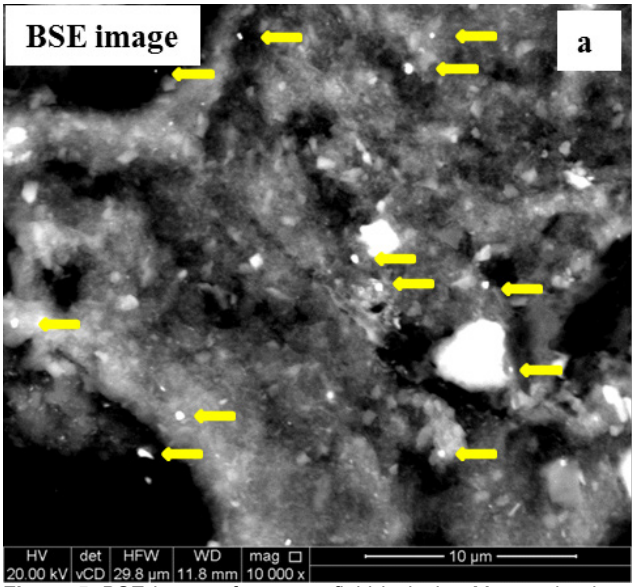

Figure 5. BSE image of an open fluid inclusion Many sub-micron Au-grains (indicated by yellow arrows) sit on sub-crystalline calcite precipitated on the inner surface of the fluid inclusion.

some as small as 100 nm can be observed in the BSE image. These are attached to the surface of semi-crystalline calcite that coats the inner surface of the fluid inclusions.

5 LA-ICP-MS analyses

The reproducibility of analyses for Au and Ag is well over 100% due to these elements being present as particles in the fluid inclusions and not dissolved in solution. The particulate signal for Au and Ag can be seen from the ablation signal where Au and Ag are seen as spikes, contrasting with the smooth asymmetric signal for Na and K that are present in solution. Part of the variability in concentration is due to the inevitability that the sequential measurement of isotopes, using quadrapole mass spectrometers, will result in an unknown number of particles passing through the ICP-MS without being measured, hence the reduction in the precision of the analyses and concentrations that are too low. In addition, if the particles were precipitated before entrapment, the number trapped in the fluid inclusions will vary immensely between different fluid inclusions.

The range in Au and Ag analyses can be seen in Figure 6, where Ag-Au pairs are plotted and show that there is an almost 3 orders of magnitude range in values for Au and Ag. The concentrations are from ablation of single unopened fluid inclusions and are all in excess of the detection limits shown for the analysis of Au and Ag in fluid inclusions. Using this data the average concentration for Ag is 32 ppm and Au 41 ppm, but as not all of the Au-Ag particles will have been detected by the ICP-MS we suggest the true concentration of Au and Ag in the fluid inclusions may be towards the higher end of values recorded, c. 100 ppm.

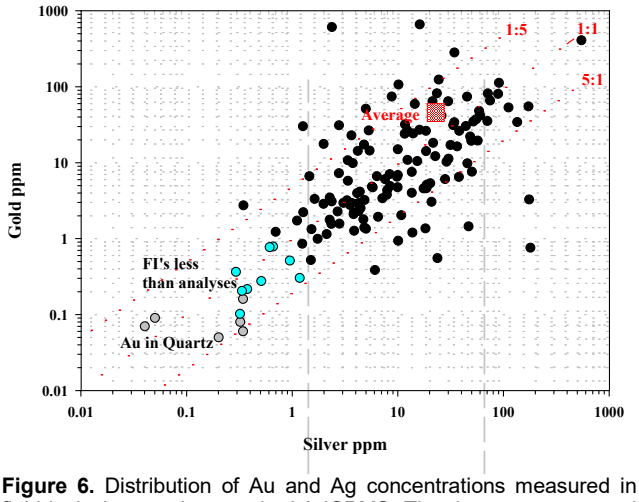

Figure 6. Distribution of Au and Ag concentrations measured in fluid inclusions and quartz by LA-ICPMS. The data covers several orders of magnitude and likely reflects missing heterogeneous trapping of Au-Ag particles and particles that were not analysed in the ICP-MS.

A number of LA-ICP-MS analysis were made on the quartz matrix, but the Au and Ag concentrations are well below 0.5 ppm, confirming all Au and Ag resides in the fluid inclusions. The lack of Au and Ag when ablating the quartz also shows there is no surface contamination affecting the analyses of Au-Ag despite some fluid inclusions being close to the surface.

6 Discussion

The suggestion that gold can be transported as colloids has been proposed for some time (Herrington and Wilkinson 1993; Saunders 1990, 2012) as a means of transporting gold at elevated concentrations greater than is possible in solution. Although there are other constraints on forming giant epithermal gold deposits (Richards 2013) "bonanza" grades (Saunders and Schoenley 1995; Saunders 2012) are often associated with the observation of colloidal gold in the ore veins. Direct evidence of gold colloids in hydrothermal fluids, was first reported by Gartman et al. (2018) in the boiled black smoker fluids from the Lau Basin. Our observation of sub-micron gold particles being carried in a mineralizing fluid, and trapped in fluid inclusions, is consistent with this process.

The concentrations determined here (average Au 41ppm, Ag 32 ppm) are substantially above any reported analyses, or of any theoretical concentrations (Gammons and Williams-Jones 1997; Hurtig and Williams-Jones 2015). However, experimental results of liquid vapour partitioning (Zajacz et al. 2017) at closer to magmatic temperatures show the vapor phase can attain concentrations of a few 10's ppm Au but still below the values determined in this study.

It is clear that the Au-Ag particles did not precipitate from the fluid once it was trapped as fluid inclusions. The heterogeneity of the LA-ICP-MS analyses and the high concentration of Au and Ag, which can exceed the concentrations of the alkali and alkaline earth elements that are normally most dominant in hydrothermal fluids, is not feasible. Instead we propose that the particulates trapped in the inclusions are the consequence of fluid boiling elsewhere in the mineralizing system and have been accidentally trapped. The fluids and solids were trapped between rapidly growing fibrous quartz, which would create structures similar to fluid-filled tubes, during periods when the fluid was supersaturated with respect to quartz. As pulses of hot low salinity fluid and/or vapor ascended from deeper in the mineralizing system, it cooled due to adiabatic expansion, which led to a decrease in silica solubility as well as that of the metals in solution. Reduction in pressure leading to boiling is also likely to have been a major factor in precipitating different minerals. The calcite coating of the inner walls of the inclusions together with the precipitation of sulphates and sulfides is reminiscent of the associations observed in vein systems with large boiling zones. In the quartz crystals studied, the fluid inclusions provide evidence of pressure transitions from near lithostatic to near hydrostatic conditions, and the presence of flashed fluids (fluids which on rapid pressure drop instantaneously convert to low density vapour) indicates, that there were occasionally periods of transient sub-hydrostatic pressures. Fluids were boiling during these pressure fluctuations and cooled to lower temperatures which is likely to be the reason for the precipitation of the more massive sulfide ores in other parts of the vein systems.

Numerous examples of base-metal and Au, or Au dominated deposits are present in the Biga Peninsula of NW Turkey, and the fluid inclusion characteristics of those Au-deposits are similar to the low salinity fluids in this study. Other deposits that are base-metal resources, contain fluid inclusions with higher salinities, but also with the same low salinity fluid as in Arapucandere. The previous interpretation that this low salinity fluid had a meteoric origin is clearly incorrect as we have shown. This is most likely a condensed low density vapour or low salinity fluid which separated from more saline magmatic fluids at depth expanding to cooler shallower levels. The presence of particulate gold at high concentrations in these fluids shows their importance in the mineralizing process as they appear to be the main transporter of gold.

Thus, whilst the Arapucandere deposit is a minor one, the direct observation and transportation of Au and Ag in particulate form, and the high concentrations possible, is a significant result with implications for porphyry and epithermal mineralization.

Acknowledgements

The authors thank Larryn Diamond and Antonin Richard for their helpful comments. Richard Walshaw's technical expertise greatly enhanced the quality of the SEM and CL imaging.

References

Bozkaya G. Banks DA (2015) Physico-chemical controls on ore deposition in the Arapucandere Pb-Zn-Cu-precious metal deposit, Biga Peninsula, NW Turkey. Ore Geol Rev 66:65-81.

Gammons CH, Williams-Jones AE (1997) Chemical mobility of gold in the porphyry-epithermal environment. Econ Geol 92:45-59.

Gartman A, Hannington M, Jamieson JW, Peterkin B, Garbe-Schonberg D, Findlay AJ, Fuchs S, Kwasnitschka T (2018) Boiling induced formation of colloidal gold in black smoker hydrothermal fluids. Geology 46:39-42.

Herrington RJ, Wilkinson JJ (1993) Colloidal gold and silica in mesothermal vein systems. Geology 21:539-542.

Richards JP (2013) Giant ore deposits formed by optimal alignments and combinations of geological processes. Nat. Geosci 6:911-916.

Hurtig NC, Williams-Jones AE (2015) Porphyry-epithermal Au-Ag-Mo ore formation by vapor-like fluids: New insights from geochemical modelling. Geology 43:587-590.

Saunders JA (1990) Colloidal transport of gold and silica in epithermal precious-metal systems: Evidence from the Sleeper deposit, Nevada. Geology 18:757-760.

Saunders JA, Schoenly PA (1995) Boiling, colloidal nucleation and aggregation, and the genesis of bonanza Au-Ag ores of the Sleeper deposit, Nevada. Mineral Deposita 30:199-210.

Saunders JA (2012) Textural evidence of episodic introduction of metallic nanoparticles into bonanza epithermal ores. Minerals 2:228-243.

Zajacz Z, Candela PA, Piccoli PM (2017) The partitioning of Cu, Au and Mo between liquid and vapor at magmatic temperatures and its implication for the genesis of magmatic-hydrothermal ore deposits. Geochim Cosmochim Acta 207:81-101.

Thermal peak detected in gold-bearing shear zones by a thermo-structural study: a new tool to retrieve fluid flow?

Gaétan Link, Olivier Vanderhaeghe, Didier Béziat, Michel de Saint Blanquat, Margot Munoz, Guillaume Estrade
Université de Toulouse, IRD, CNES (Toulouse, France)

Laurent Guillou-Frottier, Eric Gloaguen, Abdeltif Lahfid, Jérémie Melleton
Université d'Orléans, CNRS, BRGM (Orléans, France)

Abstract. Gold mineralization in the northern part of the Canigou massif (Eastern Pyrenees, France) are localized along regional-scale shear zones. These structures connect the upper metapelitic greenschist facies unit (suprastructure) to the lower migmatitic unit (infrastructure) and are attributed to the late-Variscan tectonic evolution transposing earlier structures. Raman spectroscopy of carbonaceous materials (RSCM) approach documents thermal anomalies in these shear zones with a temperature peak [20 – 100 °C] above the host rocks values. These thermal anomalies are interpreted as recording the upward circulation of a hot fluids. These data point to gold mobilization and transfer controlled by localized deformation and fluid flow at the end of the Variscan orogeny. The nature and origin of the mineralizing fluids, the source(s) of gold, and the mechanisms of ore mobilization-transfer-deposition remain to be determined.

1 Introduction

Fluid flow is known to modify mechanical (Sibson 1992) and thermodynamic features of the crust (Ague 2014). Chemical mass transfer and heat transfer are associated with fluid circulation (Yardley 2005). However, the regional thermal influence of fluid flow remains difficult to retrieve (Ague 2014).

Gold deposits are good evidence of crustal fluid flow. They can provide insights into crustal evolution processes, such as fluid evolution or mass transfer (Philips and Powell 2009). The orogenic gold model implies that metamorphic fluids from the lower crust move upward through trans-crustal shear zones and form gold deposits in the middle and upper crust (Groves et al. 1998; Goldfarb and Groves 2015). However, lower crust levels, where fluids and metal could come from, are rarely exhumed near gold deposits, so their source is difficult to retrieve (Thomkins 2013).

In orogens, metamorphic domes are structures where both upper and lower parts of the crust are exhumed (Whitney et al. 2004). Therefore, they are good targets to retrieve the origin and pathways of former mineralized fluids. Thus, we focused our study on the Canigou dome, in the Axial Zone of the Eastern Pyrenees (France), a late-Variscan metamorphic dome, where the lower levels of the crust are exhumed (Gibson and Bickle 1994; Barbey et al. 2001; Aguilar et al. 2015). Gold mineralizations have been described in the upper crustal levels of this dome (Blès and Costargent 1985; Polizzi 1990).

2 Geological settings of the Canigou massif

The Canigou massif is located in the Axial Zone of the Pyrenees, where the Variscan basement is exposed. The area consists of a metamorphic dome cored by migmatites designated as the infrastructure with a foliation delineating the shape of the dome. The dome is surrounded by Ediacarian-Cambrian metasediments dominated by metapelites designated as the suprastructure, marked by folding of an $S_0/S_{1\text{-}2}$ foliation into upright F3 folds associated with the development of a subvertical axial planar S_3 schistosity. The contact between suprastructure and infrastructure is marked by a zone of transposition interpreted to represent strain partitioning along an attachment zone (Cochelin et al. 2017) (Fig. 1).

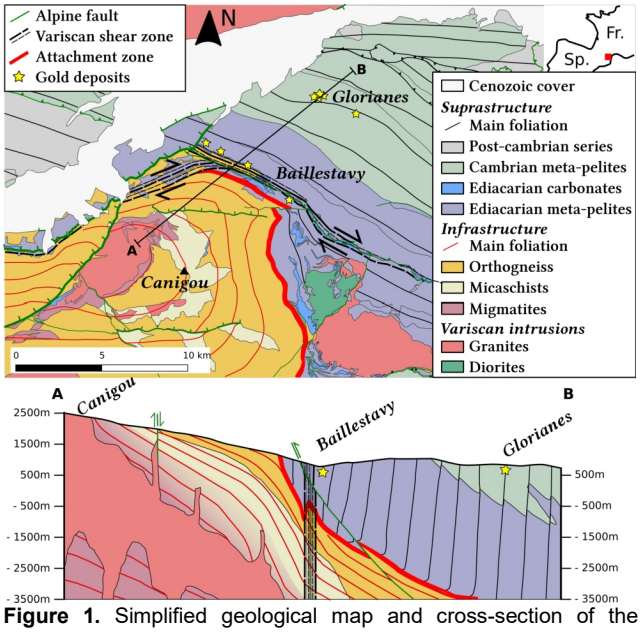

Figure 1. Simplified geological map and cross-section of the Canigou dome and position of main gold deposits.

In the suprastructure, many gold veins have been described (Blès and Costargent 1985; Polizzi 1990). They are localized along vertical retrogressive mylonite zones (Baillestavy) and reverse faults zones (Glorianes), attributed to the last Variscan deformation stages (Blès and Costargent 1985; Polizzi 1990). The

gold veins are mainly filled with siderite, quartz and arsenopyrite. Native gold (electrum) is present in arsenopyrite-filled fractures (Polizzi 1990).

3 Structural position of gold deposits

3.1 Shear zones and migmatites of the infrastructure

The infrastructure is principally made of metapelites and orthogneiss intruded by the Canigou leucogranite, made of coarse-grained quartz-feldspars-muscovite. The presence of leucosome concordant to the syn-migmatitic foliation in textural continuity with discordant leucosomes localized along W-E trending subvertical shear zones indicates that partial melting and melt segregation were coeval with deformation (Fig. 2b). Moreover, the localization of leucogranite dykes and major quartz veins together with solid-state mylonitic deformation of the Canigou leucogranite along these shear zones suggests that magma emplacement and differentiation occurred during this deformation event (Fig. 2a).

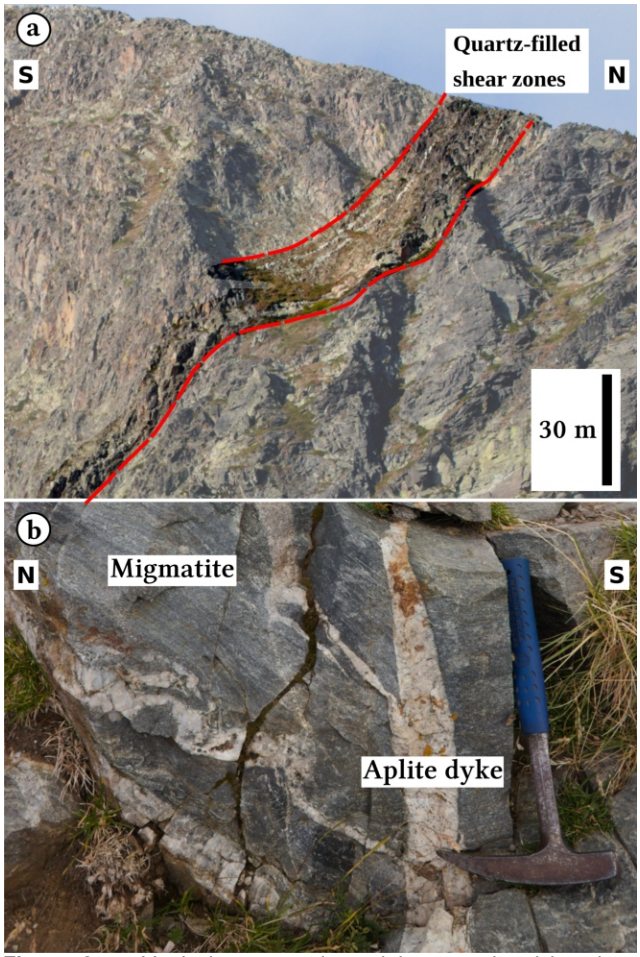

Figure 2. a. Vertical quartz vein and leucogranite dyke along vertical shear zones on the Canigou summit. **b.** Aplitic leucogranite dyke and migmatite collecting zone along vertical shear zone.

3.2 Shear zones and gold ore-bodies of the suprastructure

Near the NE edge of the Canigou dome, the Baillestavy NW-SE trending dextral shear zone crosscuts the amphibolite facies meta-pelites and carbonates and affects the attachment zone.

Many small ductile to brittle-ductile shear zones are also present in the suprastructure. They crosscut the $S_{0\text{-}1}$ and S_2 foliations and they are syn- to post-S_3. Like vertical shear zones of the infrastructure, the shear zones of the suprastructure have a W-E orientation and are mainly filled by quartz veins. The brittle-ductile shear zones are particularly concentrated in the Glorianes-Serrabona area that we designate as the Glorianes-Serrabona shear bands.

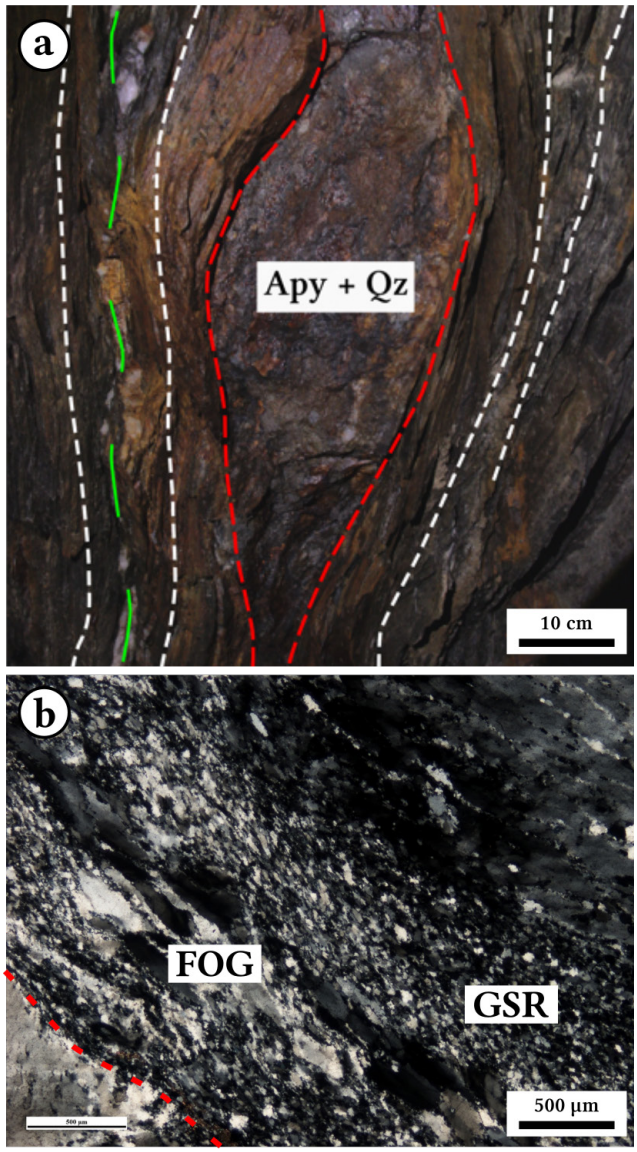

Figure 3. a. Vertical quartz-arsenopyrite vein (red) along the S_3 main foliation (white), in Glorianes gold deposit. **b.** Quartz microstructures in vertical quartz-arsenopyrite auriferous vein showing grain-size reduction (GSR) and flattened old grains (FOG); in red, contact between strongly deformed vein and weakly deformed vein.

Gold ore-bodies of the suprastructure are located along the Baillestavy shear zone and the Glorianes-Serrabona shear bands. They consist of siderite-quartz-arsenopyrite vertical veins (Fig. 3a). Microstructures of quartz show an abundant dynamic recrystallization by dislocation creep with strong grain-size reduction (GSR) and flattened old grains (FOG) (Fig. 3b). These microstructures show that the quartz deformed under ductile conditions (T > 400 °C) (Passchier and Trouw 2005). Moreover, microstructural textures show that, at least two quartz filling events occurred in the vein. Indeed, the second deformed quartz vein crosscuts the first deformed quartz vein (Fig. 3b). It suggests that fluid flow was active during the shear strain.

4 Regional thermal gradient

The regional thermal gradient has been determined by the Raman spectroscopy on carbonaceous material (RSCM) method (Beyssac et al. 2002). This geothermometer is based on the structural organization of carbonaceous material. It provides the maximum temperature reached by the rock. Previously obtained RSCM temperatures for the Axial Zone of the Pyrenees are considered to record the Variscan thermal peak (Cochelin et al. 2018). Measurements have been carried out on metapelite samples from the suprastructure and the infrastructure.

The thermal profile from the migmatitic dome core (ca. 620 ± 20 °C) and the external parts of the suprastructure (ca. 380 ± 20 °C) shows a regular decreasing gradient of ca. 30 °C/km (Fig. 4a, b). However, two thermal anomalies are present along the Baillestavy and the Glorianes-Serrabona shear bands (Fig. 4b, c). The temperature value strongly increases along these structures. It is comprised between 550 ± 37 °C and 575 ± 21 °C in the Baillestavy shear zone and between 464 ± 18 °C and 521 ± 41 °C in the Glorianes-Serrabona shear bands. They contrast with the thermal peak recorded in the surrounding rocks, where temperature reach [476 ± 21 °C – 532 ± 38 °C] and [413 ± 12 °C – 448 ± 15 °C], respectively (Fig. 4a, b). Notably, ΔT interval is very similar in both Baillestavy and Glorianes-Serrabona shear zones: [20 – 100 °C].

5 Discussion and conclusion

Temperature values obtained by RSCM approach on metapelites are consistent with petrological observations of LP/HT paragenesis. The temperature peaks identified could reflect local extrusion accommodated by conjugate faults. However, such faults have not been identified in the field. According to recent studies, shear heating may also be invoked to explain thermal anomalies identified by RSCM approach (Souche et al. 2013; Fauconnier et al. 2014). However, this process might be only valid for major crustal shear zones or supradetachments (Duprat-Oualid, pers. comm. 2018). Another possible source for anomalously high temperatures at depth may be represented by exothermic reactions during chloritization of biotite, but it

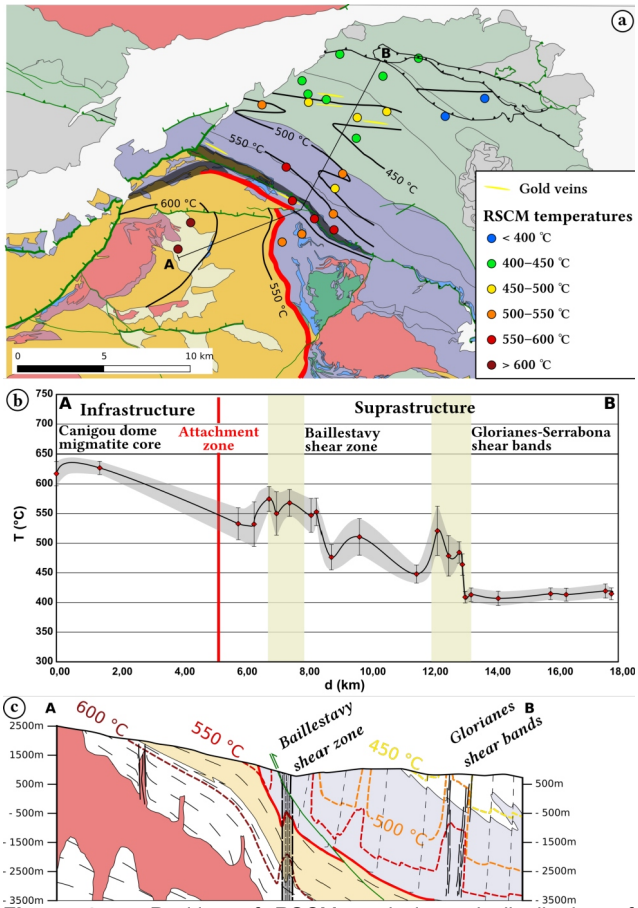

Figure 4. a. Position of RSCM analysis and distribution of isograds. Same legend as Fig. 1. **b.** Paleotemperatures obtained by RSCM along A-B cross section. Errors bars are standard deviation. **c.** Interpreted position of isograds in A-B cross section, based on RSCM datas and structural observations.

seems difficult to generate temperature anomalies reaching tens of degrees Celsius. As an alternative, we thus propose that the Baillestavy and Glorianes-Serrabona thermal anomalies reflect localized heating caused by circulation of a hot fluid in the shear zones. This interpretation is consistent with quartz microstructures in the mineralized veins, which show a deformation under ductile regime during fluid circulation.

Such fluids could originate from different sources that are not mutually exclusive. Indeed, they could represent meteoric fluids penetrating the upper crust down to the brittle-ductile transition, where they were heated before migrating upwards, as typically identified in metamorphic core complexes (Morrison and Anderson 1998; Siebenaller et al. 2013). The fluids could also be generated by dehydration metamorphic reactions as proposed for mineralizations in the Vall de Ribes district, on the south flank of the Canigou dome, where fluid inclusions revealed an H_2O-NaCl chemistry and trapping conditions under 350-400 °C and 2 kbar (Ayora et al. 1992). In that case, upwelling fluids probably incorporated gold from disseminated sulphides of the meta-sedimentary pile. Such auriferous disseminated sulphides have been observed in the Vall de Ribes district as well (Ayora and Casas 1986). Moreover, this

model involves a preexisting gold metal stock in meta-pelites and carbonates (Gaboury 2013), as proposed for the nearby Salsigne gold deposit (Montagne Noire, France) (Courjault-Radé et al. 2001). At last, the mineralizing fluids might originate from crystallization of the migmatites and granites forming the core of the Canigou dome. Constraining the origin of the mineralizing fluids requires fluid inclusion analyses.

In conclusion, our study shows that gold deposits of the Canigou massif formed during the late tectonic evolution of the Variscan orogenesis. Upward gold-forming fluid flow used vertical shear zones, which crosscut both the infrastructure and the suprastructure, as pathways. According to our structural model, the crustal thickness between gold deposits and migmatites is ca. 5 km. This contrasts with the transcrustal fault system controlling fluid flow and gold mobilization-transfer-deposition invoked in the orogenic gold model proposed by Groves et al. (1998).

By combining structural observations and RSCM data, we were able to detect the thermal signature of fluid flow along structures which were difficult to retrieve by a classical petro-structural study. Using this thermo-structural approach at a regional scale could be a useful tool for detection of ore deposits in faults and shear zones and to a better understanding of former fluid flow in the orogenic crust. It could also be a useful tool to identify areas with potential ore deposits for exploration.

Acknowledgements

This project is funded by the "*Référentiel Géologique de France (RGF) – chantier Pyrénées"* program of the BRGM (French Geological Survey).

We acknowledge Benjamin Le Bayon and Luc De Hoÿm de Marien for providing us two samples from the Canigou massif, which greatly helped us to carry out the RSCM study. We acknowledge Bryan Cochelin, Laurent Bailly, Guillaume Vic, Stefano Salvi, Stéphanie Duchêne and John Cunningham for constructive discussions.

References

Ague JJ (2014) Fluid Flow in the Deep Crust. In: Holland HD, Turekian KK (ed) Treatise on Geochemistry, 2nd edn. Elsevier, pp 203–247

Aguilar C, Liesa M, Štípská P, Schulmann K, Muñoz JA, Casas JM (2015) P–T–t–d evolution of orogenic middle crust of the Roc de Frausa Massif (Eastern Pyrenees): a result of horizontal crustal flow and Carboniferous doming? J Metam Geol 33:273–294

Ayora C, Casa J-M (1986) Strata-bound As-Au mineralization in pre-Caradocian rocks from the Vall de Ribes, Eastern Pyrenees, Spain. Miner Deposita 21:278–287

Ayora C, Ribera F, Cardellach E (1992) The Genesis of the Arsenopyrite Gold Veins from the Vall de Ribes District, Eastern Pyrenees, Spain. Econ Geol 87:1877–1896

Barbey P, Cheilletz A, Laumonier B (2001) The Canigou orthogneisses (Eastern Pyrenees, France, Spain): an Early Ordovician rapakiwi granite laccolith and its contact aureole. C R Earth Planet Sci 332:129–136

Beyssac O, Goffé B, Chopin C, Rouzaud JN, (2002) Raman spectra of carbonaceous material in metasediments: a new geothermometer. J Metam Geol 20:859–871.

Blès J-L, Costargent R (1985) Etude de l'environnement structural des minéralisations aurifères de Glorianes et Saint-Pons (Aspres nord-occidentales; Pyrénées orientales). Report 85 SGN 529 GEO, BRGM

Cochelin B, Chardon D, Denèle Y, Gumiaux C, Le Bayon B (2017) Vertical strain partitioning in hot Variscan crust: Syn-convergence escape of the Pyrenees in the Iberian-Armorican syntax. Bull Soc Geol Fr 188:39.

Cochelin B, Lemirre B, Denèle Y, de Saint Blanquat M, Lahfid A, Duchêne S (2018) Structural inheritance in the Central Pyrenees: the Variscan to Alpine tectonometamorphic evolution of the Axial Zone. J Geol Soc 175:336–351.

Courjault-Radé P, Béziat D, Munoz M, Tollon F (2001) Les concentrations en or et arsenic de la mine de Salsigne (Cabardès, Aude) : un héritage Ordovicien supérieur remobilisé à l'Hercynien ? Les Techniques de l'Industrie Minérale, 11:21–33

Fauconnier J, Labrousse L, Andersen TB, Beyssac O, Duprat-Oualid S, Yamato P (2014) Thermal structure of a major crustal shear zone, the basal thrust in the Scandinavian Caledonides. Earth Planet Sci Lett, 385:162–171.

Gaboury D (2013) Does gold in orogenic deposits come from pyrite in deeply buried carbon-rich sediments?: Insight from volatiles in fluid inclusions. Geology, 41:1207–1210. doi: 10.1130/G34788.1

Gibson RL, Bickle MJ (1994) Thermobarometric constraints on the conditions of metamorphism in the Canigou massif, Pyrenees: implications for Hercynian geothermal gradients. J Geol Soc, 151:987–997

Goldfarb RJ, Groves DI (2015) Orogenic gold: Common or evolving fluid and metal sources through time. Lithos, 255:2–26.

Groves DI, Goldfarb RJ, Gebre-Mariam M, Hagemann SG, Robert F (1998) Orogenic gold deposits: A proposed classification in the context of their crustal distribution and relationship to other gold deposit types. Ore Geol Rev, 13:7–27

Morrison J, Anderson JL (1998) Footwall refrigeration along a detachment fault: implications for the thermal evolution of core complexes. Science 279:63–66

Passchier CW, Trouw RAJ (2005) Microtectonics. Springer-Verlag, Berlin

Phillips GN, Powell R (2009) Formation of gold deposits: Review and evaluation of the continuum model. Earth Sci Rev, 94:1–21.

Polizzi S (1990) Les minéralisations sulfo-arséniées aurifères du massif des Aspres (Pyrénées orientales, France) : étude géologique et métallogénique. Dissertation, Université Paul Sabatier

Sibson RH (1992) Fault-valve behavior and the hydrostatic–lithostatic fluid pressure interface. Earth Sci Rev 32:141–144

Siebenaller L, Boiron M-C, Vanderhaeghe O, Hibsch C, Jessell MW, Andre-Mayer A-S, France-Lanord C, Photiades A (2013) Fluid record of rock exhumation across the brittle-ductile transition during formation of a Metamorphic Core Complex (Naxos Island, Cyclades, Greece). J Metam Geol 31:313-338.

Souche A, Medvedev S, Andersen TB, Dabrowski M (2013) Shear heating in extensional detachments: Implications for the thermal history of the Devonian basins of W Norway. Tectonophysics, 608:1073–1085.

Thomkins AG (2013) On the source of orogenic gold. Geology 41:1255–1256.

Whitney DI, Teyssier C, Vanderhaeghe O (2004) Gneiss domes and crustal flow. In: Whitney DI, Teyssier C, Siddoway CS (ed) Gneiss dome in orogeny. Geol Soc Am Spec Pap 380:15-26

Yardley BWD (2005) Metal concentrations in crustal fluids and their relationship to ore formation. Econ Geol 100th Anniv Spec Pap 100:613–632

REE geochemistry of the sulfides and native gold of the Olympiada deposit (Russia, Siberia)

Sergey A Silyanov, Anatoly M Sazonov
Siberian Federal University, Krasnoyarsk, Russia

Platon A Tishin
National Research Tomsk State University, Tomsk, Russia

Abstract. The paper provides data for a study of REE distribution in sulfides and native gold of the Olympiada deposit (Russia, Siberia), the largest gold producer in Russia. Pyrite, pyrrhotite, arsenopyrite, and native gold are characterized by similar patterns of distribution of lanthanides, which are close to host rock REE patterns. For antimony minerals, a different type of distribution of rare earth elements is established, with a spectrum exhibiting enrichment in some MREEs. It is assumed that gold-sulfur-arsenic mineralization is formed with involvement of the upper crust, while the formation of antimony involved mantle fluids.

1 Introduction

Due to the development of high-accuracy precision analytical methods (ICP-MS, LA-ICP-MS, SIMS, etc.), great attention is paid to the study of trace-elements in mineral deposits and their host rocks. Data for the distribution of trace elements as well as precious metals allow us to obtain information on the source of metals substance, and forms a finding of ore components in minerals and ore-forming processes in general (Goryachev et al. 2008; Guangzhou et al. 2009; Nekrasova et al. 2010; Kun et al. 2014; Volkov et al. 2016; Silyanov et al. 2018).

In this paper, we provide information on the distribution of REE in ore minerals and native gold of the Olympiada deposit, one of the largest Au deposits in Russia.

2 Geological Characteristics of Deposit

The Olympiada Au deposit is located within the Yenisei Ridge (Russia, Siberia), a 200-km-wide Neoproterozoic accretionary-collisional orogeny, extending for 700 km along the western margin of the Siberian craton. The deposit is confined to the silicate and carbonate band of the Lower Riphean Kordinskaya suite. Granitoids are distributed at 1.5 km and above from the deposit. Introduction of intrusions in the Tatar-Ishimbinskaya tectonic zone assisted in the formation of compensation synformal depressions (Innokentyevskaya and Chirimbinskaya synclines) in the contact zones of intrusions united by the antiformal rock unit (Medvezhinskaya anticline). These connected W-shaped structural elements represent the structure of the ore field. Subhorizontal shifts in the area shaped the magmatogene structure into a tectonic syncline and anticline folds.

The ore bodies are concentrated in fold hinges and parasitic folds along limbs. The micaceous-quartz-carbonate matrix of the sulfide-disseminated ores has been boudinaged, mylonite-altered and folded into minor folds up to goffering Ore minerals (main minerals – arsenopyrite, pyrite, pyrrhotite, stibnite, and native gold) form disseminations and veinlets in the host rocks.

The ores are divided into gold-arsenic and gold-arsenic-antimony ores separated spatially and temporally. The industrial ores of gold-arsenic composition have an age (Ar-Ar) of 803–758 Ma, and the gold-arsenic-antimony ores dated (Ar-Ar) at 795–660 Ma (Sazonov et al. 2019; Gibsher et al. 2019).

3 Samples and Methods

Specimens of sulfide minerals (arsenopyrite – Apy, pyrrhotite – Po, pyrite – Py and stibnite – Stb) and native gold (Au) were collected from small technological and drill samples from the Eastern section of the Olympiada deposit. The process of sample preparation is described by Silyanov et al. (2018).

Trace elements analyses were carried out using an Agilent 7500cx ICP-MS (Agilent Technologies). Before analysis, using the incremental decomposition technique the weighted sulfide probes were digested using AquaRegia. The quality of the measurements was monitored using BCR-2, BHWO, SSL-1 and other standards. The analyses were performed in Analytic Center for Natural Systems Geochemistry, Tomsk State University, Tomsk, (analysts E.V. Rabtsevich and E.I. Nikitina).

4 Results

Maximum REE concentrations were exhibited for arsenopyrite (37.04 ppm) and stibnite (41.15 ppm); pyrite, pyrrhotite and native gold have low ΣREE: 7.93, 2.72 and 1.64 ppm, respectively (Table 1). Specimens are characterized by LREE enrichment (83-99%) and a slight predominance of HREE relative to MREE (~8% vs. ~3%). In the group of LREE, La and Ce dominate. For arsenopyrite, pyrite, pyrrhotite and native gold, La prevails over Ce, while stibnite shows a reverse tendency.

Chondrite-normalized (McDonough and Sun 1995) REE profiles for sulfides and native gold are characterized by LREE-enrichment

(ΣLREE/ΣHREE=6.2-10.7) and flat HREE (Gd_N/Yb_N=1.2-2.5) patterns (Table 1 and Fig. 1). Stibnite is characterized by a distinctly different chondrite-normalized REE pattern due to the predominance of Gd, Tb and Dy (Fig.1). The sample is also characterized by elevated concentrations of La, Ce and Pr.

Table 1. Content of REE (ppm) and indicator ratios in the studied samples

Element	Stb	Apy	Po	Py	Au
La	38.817	8.100	0.551	2.006	0.445
Ce	1.775	17.604	1.308	3.100	0.758
Pr	0.085	1.527	0.100	0.297	0.060
Nd	0.067	5.333	0.357	1.161	0.196
Sm	0.015	1.118	0.092	0.260	0.037
Eu	0.005	0.191	0.015	0.055	0.010
Gd	0.062	1.039	0.086	0.264	0.035
Tb	0.016	0.156	0.013	0.043	0.006
Dy	0.275	0.920	0.078	0.276	0.040
Ho	0.003	0.173	0.016	0.060	0.008
Er	0.012	0.431	0.048	0.173	0.022
Tm	0.002	0.058	0.007	0.027	0.003
Yb	0.011	0.339	0.040	0.183	0.018
Lu	0.003	0.048	0.006	0.028	0.003
ΣREE	41.15	37.04	2.72	7.93	1.64
ΣLREE	40.74	32.56	2.32	6.56	1.46
ΣMREE	0.02	1.31	0.11	0.31	0.05
ΣHREE	0.39	3.16	0.29	1.05	0.14
ΣL/ΣH	105.75	10.29	7.90	6.24	10.72
Eu/Eu*	0.48	0.54	0.52	0.64	0.82
Ce/Ce*	0.24	1.21	1.35	0.97	1.12
Tm/Tm*	1.32	0.98	1.00	0.98	1.08
TE3	7.09	0.02	0.05	0.04	0.04
TE4	0.24	0.04	0.03	0.01	0.05
Sm/Nd	0.22	0.21	0.26	0.22	0.19

Note:
Stb – stibnite, Apy – arsenopyrite, Po – pyrrhotite, Py – pyrite, Au – gold;
$Eu/Eu^*=Eu_n/\sqrt{(Sm_n*Gd_n)}$;
$Ce/Ce^*=Ce_n/\sqrt{(La_n*Pr_n)}$;
$Tm/Tm^*=Tm_n/\sqrt{(Er_n*Yb_n)}$;
Calculation of the tetrahedral effect of REE fractioning (TE3, TE4) performed using the formulas borrowed from (Monecke et al. 2002).

For regionally metamorphosed rocks of the Kordinskaya suite (RF1kd), not affected by hydrothermal processes, all minerals considered are significantly depleted in REE (Kordinskaya suite rock composition borrowed from the work Likhanov et al. (2006), average for two specimens E-8 and E-10). The shape of the REE profiles for Apy, Po, Py, and Au are similar to the host rocks, as evidenced by substrate-normalized values of La_N/Yb_N (0.6-1.3), La_N/Sm_N (0.9-1.8), and Gd_N/Yb_N (0.6-1.3) approaching values of 1.

All analyses of sulfides and gold are characterized by negative Eu-anomalies (0.52-0.82) and slightly to moderate (or unremarkable for Py – 0.97) positive Ce-anomalies (1.12-1.35) (Table 1, Fig. 1). Stibnite exhibits negative Eu- and Ce-anomalies – 0.48 and 0.24, respectively.

Sm/Nd ratios range from 0.19 to 0.26 (Table 1). For pyrite, this ratio is close to the lower crust (LC=0.25), and for gold to the upper crust (UC=0.17), the Sm/Nd ratio of the host rocks are also close to the upper crust (RF_1kd=0.18). Other specimens are characterized by intermediate values of Sm/Nd ratio (0.21-0.22).

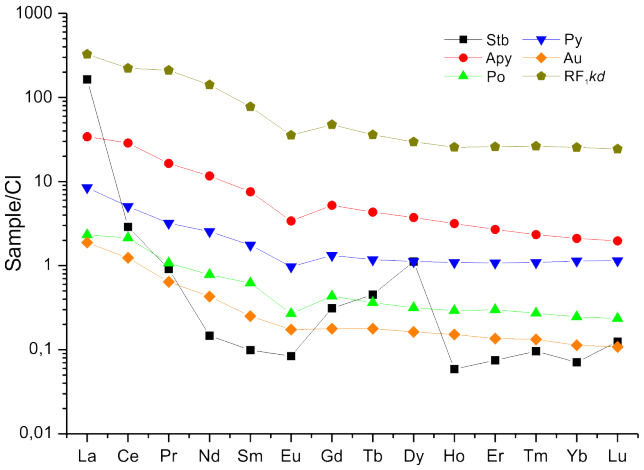

Figure 1. REE distribution in the studied samples, values scaled to chondrite (McDonough and Sun 1995). Stb – stibnite, Apy – arsenopyrite, Po – pyrrhotite, Py – pyrite, Au – gold, RF_1kd – rocks of the Kordinskaya suite (Likhanov et al. 2006, average for two specimens E-8 and E-10).

Stibnite is characterized by the presence of tetrad effect of REE fractionation (M-type) in the third (TE3=7.09) and fourth (TE4=0.24) tetrad, respectively (Table 1, Fig. 1). Fractionation of HREE in stibnite is confirmed by weak positive thulium (1.32), or negative Yb anomaly (0.69).

5 Discussion

It is thought that most of the REE in ore minerals is concentrated in fluid inclusions (Kun et al. 2014; Qiaoqin et al. 2006). Thus, the REE composition characterizes the ore-bearing fluid in equilibrium with this mineral, which allows the use of REE-characteristics in interpreting the source of fluid and its physicochemical parameters (Wang et al. 2016). However, this cannot exclude the possibility of isomorphous entry of lanthanides into the lattice of ore minerals (Qiaoqin et al. 2006), as well as the presence of REE-containing micro inclusions (Silyanov et al. 2018).

The similarity of the chondrite-normalized profiles for pyrite, pyrrhotite, arsenopyrite and native gold to signatures for the host rocks suggests an influence of the substrate on the ore-forming fluid, and an upper crust source of ore metals (Kun et al. 2014; Liu et al. 2015). This is also indicated by the Sm/Nd ratio in gold, pyrrhotite and arsenopyrite, which are close to upper crustal values. However, the high Sm/Nd ratio in pyrite does not exclude the participation of the lower crust in ore formation.

Stibnite is characterized by a different REE pattern, which, together with the geological setting of antimony mineralization in the deposit, suggests a different source. This source can be magmatic fluids, as indicated by the appearance of tetrad effects on REE fractionation in stibnite (Monecke et al. 2002).

Afanas'eva et al. (1997) came to similar conclusions when studying scheelite for these deposits (Afanas'eva

et al. 1997). It has been shown that scheelite, in association with antimony minerals, is characterized by the enrichment of MREE relative to other lanthanides. The authors suggest the participation of two fluid sources during ore formation: an early fluid depleted in REE and a later enriched REE flluid.

An interesting feature is also the appearance of the thulium anomaly, which was noted for pyrrhotite in the Panimba deposit (Yenisei Ridge, Russia) (Silyanov et al. 2018). A similar anomaly was described by Nekrasova et al. (2010) for gold in deposits of the Yenisei-East-Sayan province.

It is assumed that the behavior of europium and cerium in the hydrothermal fluids is controlled by the redox potential of the environment. The combination of positive Ce-anomaly and negative Eu-anomaly, suggests that sulfide and gold were formed under reducing conditions (Kun et al. 2014), however, the negative anomalies of both elements in stibnite suggest a change in redox potential during late stage mineral formation.

6 Conclusions

Our data show that sulfides and gold are characterized by REE patterns similar to those of their host rocks, implying that metals were derived from the host rocks and a significantly upper crust source.

At the same time, the late antimony mineralization was formed by a fluid of a different source, as evidenced by the sharply different shape of the chondrite-normalized spectrum for REE distribution in stibnite. Based on the presence of tetrad effects influencing REE fractionation, we assume that the mineral is formed with the participation of mantle fluids (Taylor and McClennan 1985; Monecke et al. 2002).

Our data on the polygenic nature of metal sources are confirmed previous studies of the isotopic composition of Pb (Savichev et al. 2006; Kryazhev 2017), Os (Naumov et al. 2015) and S (Kryazhev 2017; Gibsher et al. 2019) in ore minerals, and He in fluid inclusions in quartz and ore minerals (Naumov et al. 2015; Kryazhev 2017).

Analysis of the Eu- and Ce-anomalies indicates that the early gold-sulphide associations formed under reducing conditions; the formation of late antimony parageneses was accompanied by a change in the redox potential, as confirmed by the studies of fluid inclusions.

Acknowledgements

This work was conducted as a government task of the Ministry of Education and Science of the Russian Federation, project No. 5.2352.2017/4.6.

References

Afanas'eva ZB, Ivanova GF, Raimbault L, Miklishanskii AZ (1997) Rare-Earth Geochemistry of Rocks and Minerals from the Olimpiada Scheelite-bearing Gold Sulfide Deposit, Yenisei Ridge, Russia. Geochem Int 35(2):155-166

Gibsher NA, Sazonov AM, Travin AV, Tomilenko AA, Ponomarchuk AV, Sil'yanov SA, Nekrasova NA, Shaparenko EO, Ryabukha MA, Khomenko MO (2019) Age and duration of the formation of the Olimpiadinski gold deposit (Yenisei ridge, Russia). Geochem Int 64(5) (In press)

Goryachev NA, Golub VV, Vikent'eva OV, Bortnikov NS, Prokof'ev VYu, Alpatov VA (2008) The world-class Natalka gold deposit, northeast Russia: REE patterns, fluid inclusions, stable oxygen isotopes, and formation conditions of ore. Geol of Ore Deposits 50(5):362-390

Guangzhou M, Renmin H, Jianfeng G, Weiqiang L, Kuidong Z, Guangming L, Huijuan L (2009) Existing forms of REE in gold-bearing pyrite of the Jinshan gold deposit, Jiangxi Province, China. J Rare Earth 27(6):1079-1087

Kryazhev SG (2017) Genetic models and criteria for the prediction of gold deposits in carbon-terrigenous complexes. Dissertation, Central Research Institute of Geological Prospecting for Base and Precious Metals

Kun L, Ruidong Y, Wenyong C, Rui L, Ping T (2014) Trace element and REE geochemistry of the Zhewang gold deposit, southeastern Guizhou Province, China. Chin J Geochem 33:109-118

Likhanov II, Reverdatto VV, Vershinin AE (2006) Geochemical evidences for protolith origin of Fe-and Al-rich metapelites from Kuznetsk Alatau and Yenisey Ridge. Russ Geol Geophys 47(1):120-133

Liu J, Dai H, Zhai D, Wang J, Wang Y, Yang L, Mao G, Liu X, Liao Y, Yu C, Li Q (2015) Geological and geochemical characteristics and formation mechanisms of the Zhaishang Carlin-like type gold deposit, western Qinling Mountains, China. Ore Geol Rev 64:273-298

McDonough WF, Sun SS (1995) The composition of the Earth. Chem Geol 120:223-253

Monecke T, Kempe U, Monecke J, Sals M, Wolf D (2002) Tetrad effect in rare earth element distribution patterns: A method of quantification with application to rock and mineral samples from granite-related rare metal deposits. Geochim Cosmochim Acta 66(7):1185-1196

Naumov EA, Borisenko AS, Nevolko PA, Kovalev KR, Tessalina S, Sazonov AM, Savichev AA, Zvyagina EA (2015) Gold-sulfide (Au-As) Deposits of the Yenisei Ridge (Russia): Age, Sources of Metals and Nature of Fluids. Proceeding of the 13 Biennial SGA Meeting 165-168

Nekrasova AN, Nikolaev LA, Milyaev SA, Yablokova SV (2010) First data on the distribution of REE, Li, Rb, Cs, Sr, Ba in native gold deposits of the main gold-bearing provinces of Russia. Dokl Earth Sci 432(5):660-663

Qiaoqin X, Xiaochun X, Xiaoxuan L, Tianhu C, Sanming L (2006) Rare Earth Elements Geochemistry of Laowan Gold Deposit in Henan Province: Trace to Source of Ore-Forming Materials. J Rare Earth 24:115-120

Savichev AA, Shevchenko SS, Rozinov MI, Lokhov KI, Prasolov EM, Prilepsky EB, Kapitonov IN, Matukov DI, Berezhnaya NG, Sergeev SA (2006) Reg Geol Metallogeny 28:122-143

Sazonov AM, Zvyagina YeA, Silyanov SA, Lobanov KV, Leontyev SI, Kalinin YuA, Savichev AA, Tishin PA (2019) Ore genesis of the Olimpiada gold deposit (Russia, Yenisei ridge). GSR 1:17-43

Silyanov SA, Sazonov AM, Tishin PA, Nekrasova NA, Lobastov BM, Zvyagina YA, Ryabukha MA (2018) Geochemical indicators of the genesis of the Panimba gold deposit at the Yenisei Ridge (Siberia, Russia). GSR 3:6-21

Taylor SR and McClennan SM (1985) The Continental Crust: Its Composition and Evolution. Blackwell, Oxford 312 pp

Volkov AV, Murashov KY, Sidorov AA (2016) Geochemical peculiarities of ores from the largest Natalka gold deposit in Northeastern Russia. Dokl Earth Sci 466(2):161-164

Wang Y, Zeng Q, Zhou L, Chu S, Guo Y (2016) The sources of ore-forming material in the low-sulfidation epithermal Wulaga gold deposit, NE China: Constraints from S, Pb isotopes and REE pattern. Ore Geol Rev 76:140-151

Ore-stage calcite veins in the Carlin-type Au-deposits of the Nadaleen trend, Yukon: a new addition to the economic geologist's tool-kit.

Andrew P. Steiner, Kenneth A. Hickey
The University of British Columbia, Vancouver, Canada.

Abstract. Readily-identifiable, ultraviolet-fluorescent (UVF) calcite veins in the Carlin-type Au-deposits of the Nadaleen trend, Yukon, are linked to Au-mineralization by their spatial distribution, mineralogy, isotopic signature and chemistry. They offer exciting opportunities to study the evolution of Carlin-type ore fluids and can be used to aid exploration for these typically large, high-grade deposits. UVF veins cut fault fabrics associated with thrusting and folding, providing age constraints relative to deformation. U-Pb dating of UVF calcite provides a preliminary Eocene Au-mineralization age, which is long after any known regional magmatism, suggesting an amagmatic genesis. The orientation of UVF veins provide support for a vertically-focused ore fluid-flow regime that exploited pre-existing fold-fracture networks that parallel steeply-plunging fold hinges. UVF calcite likely formed as a product of decarbonatization of host limestones during the sulfidation reaction that deposited the Au.

1 Introduction

Carlin-type Au-deposits (CTGDs) are epigenetic carbonate-replacement deposits named after the large high-grade occurrences in northern Nevada (Cline et al. 2005). The host rocks to CTGDs are dominantly sedimentary carbonate rocks within exhumed, inverted basins (Cline et al. 2005). Decarbonatization (removal of carbonate) and subsequent silicification and argilliization of carbonate host rocks are the most common alteration indicators, along with late ore-stage mineralization of realgar, orpiment and calcite, and associated geochemical enrichments in Sb, Hg, Tl and particularly As (Cline et al. 2005). Gold occurs as sub-micron particles within the rims of As-rich pyrite, and is thought to be deposited via sulfidation of an Fe-rich wall-rock by a fluid carrying Au as bi-sulfide complexes (Cline et al. 2005). Despite their economic significance, the genesis of CTGDs is still poorly understood (Muntean et al. 2011, Ilchik and Barton, 1997).

Calcite veins are generally considered unimportant in CTGDs as they do not host any Au. However, it has been previously suggested that some calcite veins may be genetically related to Au-mineralization based on the presence of realgar, C and O stable isotope signatures, and/or trace-element enrichment relative to background values (e.g. Hofstra and Cline, 2000; Vaughan et al. 2016). Difficulty in recognizing these veins has hindered attempts to assess their significance. Here we present evidence for ore-stage calcite veins that fluoresce under short-wave ultraviolet (UV) light from the Nadaleen trend CTGDs, Yukon, Canada. These UV-fluorescent (UVF) veins can be linked spatially, temporally and chemically to the Au-mineralizing event. They provide critical information on the timing of the Au-mineralizing event, the temperature of ore-fluids, salient ore-fluid controls and the physicochemical evolution of ore-fluids along the flow path. Critically, they are easy to identify in the field with a UV-lamp, allowing them to be used as an exploration tool.

2 UV-fluorescent ore-stage calcite veins

Ore-stage calcite veins fluoresce pink to orange under shortwave UV light (Fig. 1). UVF veins can exhibit homogenous, patchy, or concentrically zoned fluorescence (Fig. 1a), and frequently occur as veinlets within pre-existing non-fluorescent calcite veins (Fig. 1b). Both the density of calcite veining and calcite vein characteristics in visible light are invariant with distance from the ore-zone. Petrographically, UVF veins are indistinguishable from non-fluorescent calcite veins. They dominantly comprise blocky crystal and rarely exhibit crack-seal growth textures, such as syntaxial growth. UVF veins exhibit a bright red cathodoluminescence (CL) response, and concentric zoning is also distinguishable in CL responses.

Detailed core-logging through sixteen diamond drill-holes reveals the spatial distribution of UVF veins to be restricted to within a few metres of Au-mineralization or alteration. Therefore, UVF veins can be used as an indicator of spatial proximity to ore-stage hydrothermal fluid flow, and may be a useful vector towards ore zones. A temporal link to Au-mineralization is established through the presence of rare syntaxial co-precipitation of realgar with UVF calcite (Fig. 1c).

3 Vein chemistry

Interaction between ore-stage fluids and carbonate host-rocks in CTGD systems results in the isotopic alteration of the latter relative to rocks distal to hydrothermal activity (Barker et al. 2013). Hydrothermally altered rocks have anomalous $\delta^{13}C$ and depleted $\delta^{18}O$ signatures relative to background values (Barker et al. 2013). Figure 2 shows $\delta^{13}C$ and $\delta^{18}O$ values for calcite vein—wall-rock sample pairs drilled from two different host-limestones: the Conrad and Osiris limestones. UVF veins (shown in pink) have a $\delta^{13}C$

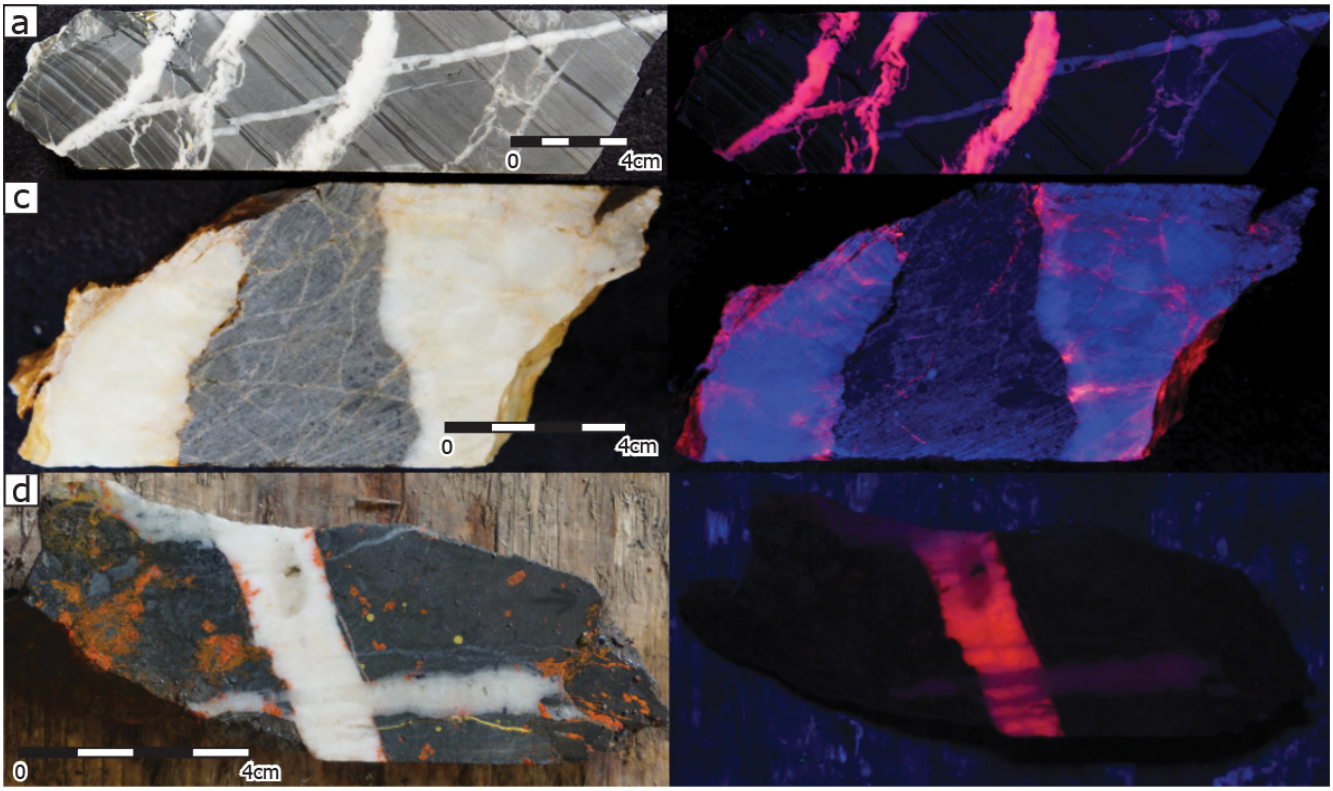

Figure 1. UVF veins from the Nadaleen trend in daylight (left) and under short-wave UV light (right). **a.** Zoned UVF veins cross-cutting patchy fluorescent veins. **c.** UVF veinlets within a non-UVF vein. **d.** Syntaxial co-growth of UVF calcite and realgar.

signature between -1 and -4‰. In $\delta^{18}O$ space, UVF veins are generally depleted relative to the adjacent wall-rock. The wall-rock values lie within the non-mineralized background range of 17 to 24‰, determined from regional non-altered samples (Moynihan et al. 2019). These $\delta^{13}C$ and $\delta^{18}O$ values suggest limited isotopic exchange between UVF vein-forming fluids and wall-rock. Since UVF veins are depleted relative to the Conrad limestone and enriched relative to the Osiris limestone, the initial $\delta^{13}C$ composition of the fluid is constrained between -1 and -4‰.

UV- and cathodo-luminescence intensity is controlled by the concentrations of Mn (a luminescence activator) and Fe (a luminescence quencher; (Rakovan and Waychunas, 1996). Non-altered host rocks and non-UVF veins have Mn and Fe concentrations of a few hundred ppm and several thousand ppm to over 1%, respectively. UVF veins are enriched in Mn by up to two orders of magnitude, with concentrations between 1000ppm and nearly 5%. Fe in UVF veins is significantly lower than non-altered wall-rock, with Fe concentrations generally <700ppm. This high Mn:Fe ratio causes the veins to fluoresce under UV light and to be cathodoluminescent. Collectively, the spatial distribution of UVF veins, their $\delta^{18}O$ and $\delta^{13}C$ signatures, their Fe and Mn chemistry and the co-precipitation of UVF calcite and realgar provide a robust genetic link to the ore-stage hydrothermal activity.

4 Timing, temperature and geological controls of ore-fluid flow

Cross-cutting relationships of UVF veins and fault fabrics indicate that Au-mineralization occurred post folding and thrusting. An Eocene U-Pb date for UVF vein calcite provides a preliminary age for hydrothermal fluid flow and mineralization along the Nadaleen trend of CTGDs. This age is consistent with apatite fission track (AFT) dates from the ore-zone interpreted to be thermal resetting temperatures since they are younger than regional cooling ages (Tucker, 2015; Hickey et al. 2014b). The temperature of vein-forming fluids can be determined from clumped isotope thermometry (CI). CI measures the "clumping" of heavy ^{18}O and ^{13}C bonds relative to predicted stochastic distribution. The difference is thermodynamically controlled and can be back-calculated to give a carbonate precipitation temperature (Huntington and Lechlar, 2015). We undertook a pilot CI study at Isolab at the University of Washington, USA, yielding a UVF calcite precipitation temperature of ~150°C determined using a modified calibration after Kluge et al. (2015) with Brand et al. (2010) parameters. AFT modelling indicates little post-Eocene exhumation, so C-O bond reordering through solid-state diffusion in UVF veins is unlikely (Stopler and Eiler, 2015). This 150°C temperature is lower than the 180-240°C main ore stage fluid temperatures determined in Nevada, but similar to fluid inclusion temperatures from late ore-stage calcite (Cline and Hofstra, 2000).

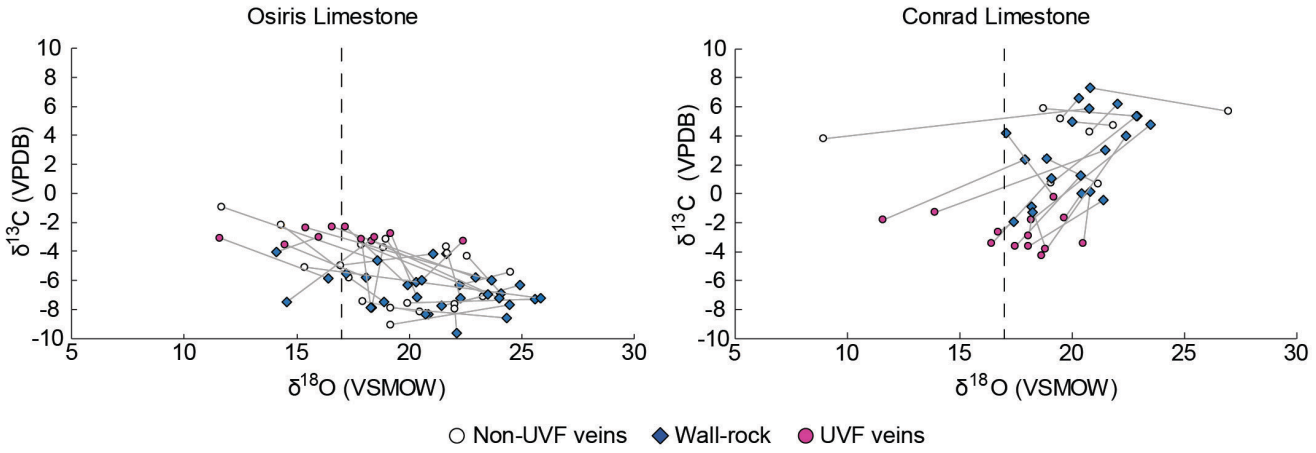

Figure 2. $\delta^{18}O$ vs $\delta^{13}C$ scatterplots for veins and wall-rock within the Osiris limestone (left) and the Conrad limestone (right) host rocks (same scales on axes of both graphs). The data is presented in pairs, with one data-point sampled from the vein, and one sampled in the adjacent wall-rock 1-10mm from the vein. These pairs are joined by a grey line. UVF veins, shown in pink, are generally depleted relative to their wall-rock pair and have a restricted $\delta^{13}C$ range between -1 and -4‰ that reflects the initial $\delta^{13}C$ composition of the vein-forming fluids.

UVF veins are predominantly either bedding-normal or bedding-parallel. This is typical of a buckle-fold—fracture network in which initial Mode-I fracturing occurred along horizontal bedding-planes and layer-parallel extension during subsequent folding of thick carbonate layers created a bedding-normal fracture set (e.g., Cosgrove, 2015). However, the age of folding is Cretaceous, and UVF veins cut fault fabrics on faults that post-date folding. Therefore, we interpret that the ore-fluids exploited a pre-existing fold-fracture network. This is consistent with the distribution and style of visible alteration in drill-core, soil As anomalies and wall-rock $\delta^{18}O$ and $\delta^{13}C$ signatures, which all indicate that fracture-controlled fluid flow is the dominant flow regime, particularly in fold-hinges. The majority of UVF veins are steeply-oriented and the folds in which they form are steeply-plunging. Thus, the fluids mainly flowed up into the deposit through this steep fracture-network.

5 Genetic model for UVF vein formation

Mn in the vein-forming fluids is thought to have been derived from decarbonatization (dissolution) of host limestones by acidic ore-fluids. Micro X-ray fluorescence element maps show that Mn is depleted in decalcified zones, which is consistent with previous observations from the CTGDs in Nevada (Vaughan et al. 2016; Cail and Cline, 2001). Gold deposition accompanies decarbonatization via the sulfidation of Fe released from the dissolving carbonate. Decarbonatization, therefore, results in a Ca- and Mn-depleted, Au-enriched, carbonate dissolution zone (CDZ), and a discharging, Ca- and Mn-enriched, hydrothermal fluid (Fig. 3). The precipitation of UVF calcite outside the CDZ likely reflect some physicochemical change in the fluid, possibly CO_2 degassing. This change causes calcite to become insoluble and the ore fluid switches from dissolving calcite to precipitating calcite. Where this fluid flows pervasively through the carbonate host rock, it precipitates Mn-rich calcite as pseudomorphs of existing calcite to form the carbonate replacement zone (CRZ; Vaughan et al. 2016). Fluids that travel further outboard of the CRZ by exploiting pre-existing fracture networks deposit UVF calcite in veins.

UVF veins are largely representative of a fold-fracture network, yet formed long after folding (>30 Myr). This suggests that the majority of UVF calcite grew as pseudomorphs of existing calcite. The observation that the density of veining does not increase towards dissolution zones is additional evidence for the replacement of pre-existing veins rather than the formation of a new CTGD-related fracture network. However, the presence of concentric luminescent zoning and syntaxial co-growth of UVF calcite with realgar indicate that some primary UVF calcite growth did occur. We propose that a minor deformation event re-fractured existing veins owing to the rheological contrast between vein and wall-rock. The Mn-rich fluids used these small fractures to travel beyond the CRZ while pseudomorphing adjacent calcite crystals, and precipitated new crystals in any open fracture spaces.

6 Implications

Our preliminary Eocene age for Au-mineralization at Nadeleen is nearly 20 Myr after the last episode of magmatism in the Selwyn basin (Kingston et al. 2010), suggesting that gold is unlikely to be sourced directly from magmas, as has been previously suggested for the deposits in Nevada (Ressel and Henry, 2006; Muntean et al. 2011). The vertically-focused, fracture-controlled fluid-flow in the Nadaleen trend is also different to the CTGDs in Nevada, where lateral fluid flow through confined aquifers was dominant (Hickey et al. 2014a). These differences highlight that the structural framework prior to Au-mineralization is important for promoting fluid flow into a deposit, and that magmatism perhaps is not an essential component in CTGD genetic models.

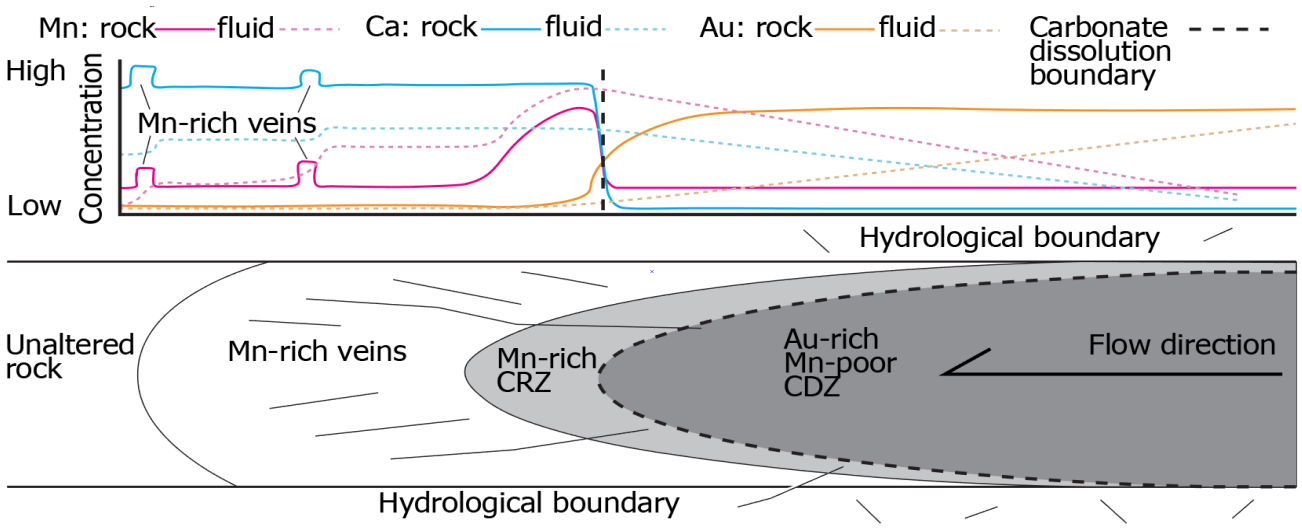

Figure 3. Idealized physicochemical evolution of the Carlin ore-fluids at Nadaleen (after Vaughan et al., 2016). Changes in the relative Mn, Ca and Au content of both rock and fluid as a result of fluid:rock interaction are shown above. The dashed black line represents the boundary between calcite solubility and insolubility in the ore-fluids

Acknowledgements

Our sincerest thanks to Julia Lane and Adam Coulter of ATAC Resources Limited for their logistical support, to Daniel Schrader and Saadan Khalid as field assistants, and to Barrick Gold Corporation for in-field support. Thank you to Kate Huntington and Andy Schauer at Isolab, University of Washington, for the clumped isotope analyses, to Greg Dipple and Frances Jones for assistance with stable isotope samples, and to Troy Rasbury and Katie Wooton for collaborating on the U-Pb dating at Stony Brook University. Project funding was provided by Natural Resources Canada through their Targeted Geoscience Initiative (TGI), the Mitacs Accelerate Program, the Society of Economic Geologists Foundation's Graduate Student Fellowship and Student Research Grant, and ATAC Resources Ltd.

References

Barker SLL, Dipple GM, Hickey KA, Lepore WA & Vaughan JR (2013) Applying stable isotopes to mineral exploration: teaching an old dog new tricks. Econ Geol 108: 1-9.

Brand WA, Assonov SS, Coplen TB (2010) Correction for the 17O interference in δ(13C) measurements when analyzing CO2 with stable isotope mass spectrometry (IUPAC Technical Report). Pure and Appl Chem 82(8):1719-1733.

Cail TL, Cline JS (200) Alteration associated with gold deposition at the Getchell Carlin-type gold deposit, north-central Nevada. Econ Geol 96:1343-1359.

Cline JS, Hofstra AH, Tosdal RM, Muntean, J, Hickey KA (2005) Carlin-type Gold Deposits in Nevada, USA: Critical Geologic Characteristics and Viable Models. In: Hedenquist JW, Thompson JHF, Goldfarb RJ, Richards JP (eds.) Econ Geol 100th Anniv Vol: pp 451-481.

Cosgrove JW (2015) The association of folds and fractures and the link between folding, fracturing and fluid flow during the evolution of a fold–thrust belt: a brief review. Geol Soc, London, Spec Publ 421:421-11.

Hickey KA, Ahmed AD, Barker SLL, Leonardson R (2014a) Fault-controlled lateral fluid flow underneath and into a Carlin-type gold deposit: Isotopic and geochemical footprints. Econ Geol 109: 1431-1460.

Hickey KA, Barker SLL, Dipple GM, Arehart GB, Donelick RA (2014b) The brevity of hydrothermal fluid flow revealed by thermal halos around giant gold deposits: Implications for Carlin-type gold systems. Econ Geol 109:1461-1487.

Hofstra AH, Cline JS (2000) Characteristics and models for Carlin-type gold deposits. Rev Econ Geol 13: 163-220.

Huntington KW, Lechler, AR (2015) Carbonate clumped isotope thermometry in continental tectonics. Tectonophys 647: 1-20.

Ilchik RP, Barton MD (1997) An amagmatic origin of Carlin-type gold deposits. Econ Geol 92:269-288.

Kingston S, Mortensen JK, Dumala M, Gabites J (2010) Ar-Ar geochronology and Pb isotopic constraints on the origin of the Rau gold-rich carbonate replacement deposit, central Yukon. In: Macfarlane KE, Weston LH, Blackburn LR (eds.) Yukon explor and geol 2009. Yukon Geological Survey, Whitehorse, Yukon, pp. 213–222.

Kluge T, John CM, Jourdan AL, Davis S, Crawshaw J. (2015) Laboratory calibration of the calcium carbonate clumped isotope thermometer in the 25–250 C temperature range. Geochim et Cosmochim Acta 157:213-227.

Moynihan DP, Strauss JV, Nelson LL, Padget CD (2019) Upper Windermere Supergroup and the transition from rifting to continent-margin sedimentation, Nadaleen River area, northern Canadian Cordillera. Geol Soc Am Bull (in press)

Muntean JL, Cline JS, Simon AC, Longo AA (2011) Magmatic–hydrothermal origin of Nevada's Carlin-type gold deposits. Nat Geosci 4(2):122.

Rakovan J, Waychunas G (1996). Luminescence in minerals. Mineral Rec, 27(1):7.

Ressel MW and Henry CD (2006) Igneous geology of the Carlin trend, Nevada: Development of the Eocene plutonic complex and significance for Carlin-type gold deposits. Econ Geol 101(2):347-383.

Stopler DA, Eiler JM (2015) The kinetics of solid-state isotope-exchange reactions for clumped isotopes: A study of inorganic calcites and apatites from natural and experimental samples. Am J of Sci 315(5):363-411.

Tucker MJ (2015) Geology, Mineralization and Geochronology of the Conrad Zone Carlin-type gold prospect, East-Central Yukon Territory, Canada. MSc thesis, University of British Columbia

Vaughan JR, Hickey KA, Barker SLL (2016) Isotopic, chemical, and textural evidence for pervasive calcite dissolution and precipitation accompanying hydrothermal fluid flow in low-temperature, carbonate-hosted, gold systems. Econ Geol 111:1127-1157.